NOTICE

The quality of this microform is heavily dependent upon the quality of the original thesis submitted for microfilming. Every effort has been made to ensure the highest quality of reproduction possible.

If pages are missing, contact the university which granted the degree.

Some pages may have indistinct print especially if the original pages were typed with a poor typewriter ribbon or if the university sent us an inferior photocopy.

Previously copyrighted materials (journal articles, published tests, etc.) are not filmed.

Reproduction in full or in part of this microform is governed by the Canadian Copyright Act, R.S.C. 1970, c. C-30.

AVIS

La qualité de cette microforme dépend grandement de la qualité de la thèse soumise au microfilmage. Nous avons tout fait pour assurer une qualité supérieure de reproduction.

S'il manque des pages, veuillez communiquer avec l'université qui a conféré le grade.

La qualité d'impression de certaines pages peut laisser à désirer, surtout si les pages originales ont été dactylographiées à l'aide d'un ruban usé ou si l'université nous a fait parvenir une photocopie de qualité inférieure.

Les documents qui font déjà l'objet d'un droit d'auteur (articles de revue, tests publiés, etc.) ne sont pas microfilmés.

La reproduction, même partielle, de cette microforme est soumise à la Loi canadienne sur le droit d'auteur, SRC 1970, c. C-30.

Canada

Investigation of the Effect of Flux Cutting on Magnetic Behaviour in Hollow Cylindrical Geometry

by

Andrzej Golebiowski

Thesis submitted to the School of Graduate Studies and Research

of the University of Ottawa in partial fulfilment

of the requirements for the degree

of Master of Science in Physics

Physics Department

Science and Engineering Faculty

University of Ottawa

Ottawa, Canada

January, 1988

ISBN 0-315-46770-3

UNIVERSITÉ D'OTTAWA
UNIVERSITY OF OTTAWA

AKNOWLEDGEMENTS

I would like to express my gratitude to Dr. Marcel A. R. LeBlanc for the huge amount of work, excellent supervision, encouragement and the financial support he provided that greatly contributed to the completion of this project.

I would like to thank the members of the supporting staff for their contribution in manufacturing and assembling the setup used in this project.

Contents

List of Figures

Chapter 1

1.1 Background Discussion

The magnetic response of type II superconductors when subjected to varying external magnetic fields has attracted the interest of researchers for many years and continues to offer many challenging problems. The magnetic behaviour of non magnetic materials in the superconducting state;

- yields information on the dependence of the bulk and surface critical current densities on temperature and magnetic flux density,
- sheds light on the interaction of the flux lines with each other, with the pinning sites and with the surface of the sample,
- provides important data for applications.

In particular, the magnitude of the hysteresis losses and their dependence on the strength of the bias magnetic field as well as on the amplitude, the frequency and the orientation, with respect to the sample, of the varying magnetic field plays an important role in most technological considerations.

Although the variety of magnetic behaviour exhibited by the "classical" low T_c type II superconductors under varying magnetic fields is not yet completely documented and far from fully understood, the focus of attention has now turned to the newly discovered high T_c ceramic materials. Eventually, a careful comparison of the similarities and differences in the magnetic behaviour of these new materials with that of their low T_c brothers should shed light on the fundamental properties and nature of both categories of substances. In this thesis we report on an investigation of flux cutting phenomena in a "low" T_c specimen. Measurements are under way in our laboratory to study these processes in high T_c samples.

1.2 Flux Transport and Flux Cutting Regimes

1.2.1 General Outline

The entry and migration of magnetic flux into type II superconductors as the external magnetic field is applied and the exit of magnetic flux lines from the specimen as the external magnetic field is removed has been most extensively studied in a very special situation, namely, in the case where the supercurrents flow transverse to the local magnetic flux density. This regime corresponds to that encountered in electromagnets, solenoids, coils, transformers etc. of standard construction. This may explain the almost exclusive preoccupation of workers with this specific regime. In these devices, the current flowing in any one segment of the assembly contributes

to the magnetic field produced by the device while bathing in an ambient magnetic field generated by the currents flowing in the neighbouring elements. In the standard arrangements exploited for these pieces of hardware, magnetic field which is produced is everywhere orthogonal to the configuration of the currents which create and sustain it.

In these circumstances, changes of the current and magnetic field are accompanied by the transport of magnetic flux lines into or out of the individual segments as the surface barriers are surmounted and the opposition of the pinning sites to these displacements is overcome. When the rate of migration of flux lines is appreciable, viscous drag can play an important role in the mechanism of energy dissipation.

A more general framework however can be envisaged and implemented where the electric current density $\vec{j}$ is made to flow with a significant component $j_{\|}$ directed along the local magnetic flux density. The physics of electromagnetism expressed by Maxwell's equation,

$$\nabla \times \vec{B} = \mu_0 \vec{j}$$

dictates that the relative orientation of adjacent sheets of flux lines must vary spatially. Under these circumstances, when $j_{\|}$, the component of $\vec{j}$ flowing along the flux lines, hence the angle between adjacent sheets of flux lines, exceeds threshold values, a new process is believed to arise. The lattice of flux lines can no longer retain its integrity and becomes unstable. A phenomenon called flux cutting is now thought to take place whereby the orientation and the density of the flux lines undergoes a radical transformation. Any such modification of orientation and density of flux lines leads to energy dissipation. In chapter 3 of this thesis we will describe two quasi macroscopic pictures of the details of the flux cutting process which have

been proposed in the literature [1,2,3,10,15]. In chapter 4 we will report on some of our observations and show how these provide unambiguous evidence for a counterflow of flux lines under some circumstances where flux cutting is taking place. The proposed models are consistent with and can readily be exploited to account for this novel feature of countermoving sheets of flux lines.

1.2.2 Flux Cutting Regime

Flux cutting is made to occur by causing a sufficiently strong component of the current to flow along the direction of the flux lines. The current can be introduced into the superconductor via leads attached to it and connected to an external source. For instance, the specimen can consist of a single straight wire or ribbon immersed in an externally applied magnetic field which is directed along the length of the sample and along the flow of the impressed current. It was this arrangement, which was the first to be exploited experimentally that led to the concept of flux cutting [6]. When the current I is raised beyond a critical value I_c, voltage probes along the superconducting wire register a potential difference, hence a resistance $R = V/I$, which depends on $\Delta I = I - I_c$ and the applied field H_a/H_{c2} where both I_c and H_{c2} vary with temperature $T < T_c$.

The steady state voltage detected along the superconducting sample carrying a constant current in a static magnetic field is referred to as a flux flow voltage. The prevailing picture of flux flow voltages can most readily be described by considering a long thin ribbon sample (planar geometry) in a uniform and static externally applied

field H_a directed parallel to the broad faces and perpendicular to the impressed current I, as shown schematically in the accompanying sketch (Figure 1(a,b)). Here I is a current per unit length of the slab along Z and Z is taken to be large compared to the thickness $W = 2X$. The profiles of the density of flux lines when $I \geq I_c$ are depicted in Figures 1 (a) and 1 (b) of the sketch. For simplicity we ignore the presence of Meissner currents (equilibrium diamagnetism) and surface barriers.

In Figure 1 (b), we present the case where the externally applied field H_a is stronger than the magnetic field $H_I = I/2$ generated outside the "infinite" slab by the transport current I. A flux flow voltage $V = E_y Y$ is visualized as arising from the continuous creation of flux lines at the surface $(-X)$ of the specimen, their steady flow across the thickness of the sample under the action of a driving Lorentz like force $\vec{F}_L = \vec{j} \times \vec{B}$, and their exit from the sample at the other surface $(+X)$. Alternatively, when $H_a < H_I$ as in Figure 1(a), a steady stream of flux lines of opposing polarity entering from both surfaces ($+X$ and $-X$) migrate towards each other and undergo mutual annihilation inside the specimen at the interface X'. In both situations, the equation

$$\vec{E} = -\vec{v}(x) \times \vec{B}(x) \tag{1}$$

expresses the relationship between the flux transport electric field $\vec{E}$, the velocity $\vec{v}$ and density $\vec{B}$ of the flux lines. By symmetry, since any Y plane is an equipotential surface, $\vec{E}_y = \hat{y} E_y$, where E_y is uniform throughout the infinite slab.

For the case of the wire in no externally applied field ($H_a = 0$), the azimuthal flux lines generated by the longitudinally impressed current I close on themselves

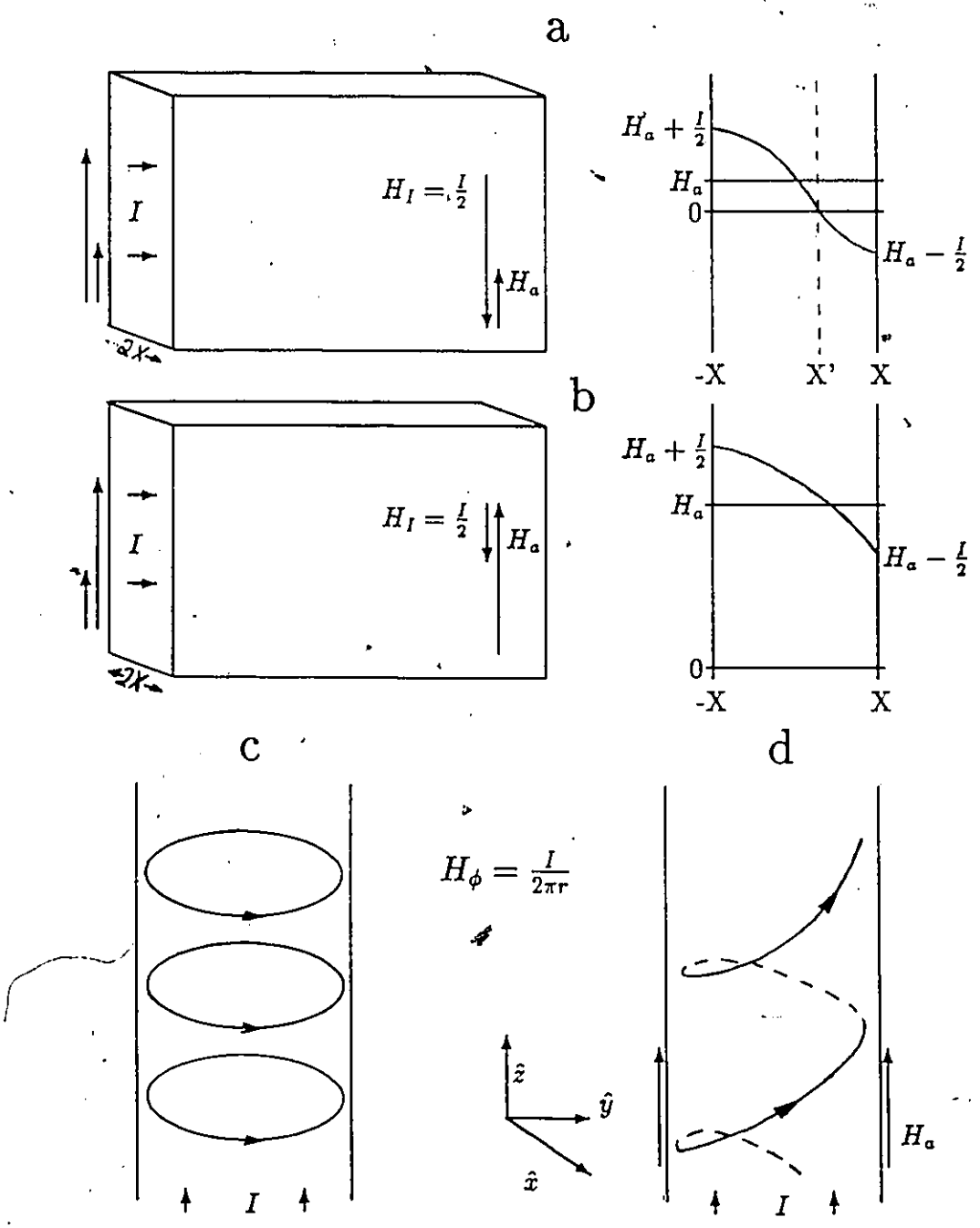

Figure 1: Magnetic flux configurations in the slab (a, b) and their analogs for cylindrical geometry (c, d).

and form vortex rings. Under the influence of the Lorentz force and line tension energy, the rings shrink radially and collapse on the axis (see Figure 1(c)). Here, equation (1) becomes

$$E_z = -v_r(r)B_\phi(r).$$

It was quickly appreciated however that the accepted picture for flux flow voltages leads to a paradox when a longitudinal magnetic field $\vec{H}_\parallel$ is present. Now, a flux line does not close on itself but forms a continuous helix extending from one end of the wire to the other as shown on Figure 1(d). A radial migration of these helical flux lines is required to account for the generation of a longitudinal electric field, hence a flux flow voltage when a stationary current exceeds I_c. This leads to the constant accumulation of the axial flux carried by each helix at the axis of the wire. Evidently, this does not constitute a steady state situation and presents a scenario which cannot be physically sustained indefinitely. Further, this picture is incompatible with the observations that the longitudinal flux density $\langle B_z \rangle$ in a wire (although paramagnetic in the sense that here $\langle B_z \rangle$ exceeds the axially applied magnetic induction $B_a = \mu_0 H_\parallel$), remains stationary when $I > I_c$ and $H_\parallel$ are maintained constant.

The idea of flux cutting was put forward by several workers to resolve the paradox. Invoking various sequences of this process, it now ensues that the azimuthal component of the lattice of helical flux lines can undergo a continuous radial transport and self annihilation at the axis of the wire while on a quasi macroscopic scale, the spatial and temporal averages of the longitudinal flux density remain unchanged. Cave et al. [6] have indeed observed that a ripple current ΔI superimposed on a steady bias current $I < I_c$ causes considerably larger variations in $\langle B_\phi \rangle$ than in $\langle B_z \rangle$

indicating that the entry and exit of the azimuthal flux component appears to be decoupled from the displacement of the longitudinal flux.

Clem [15] and Brandt [3,2,1] proposed an alternative picture where right-handed helical flux lines (see Figure 1(d)) are continuously nucleated at the surface, penetrate radially into the wire and shrink to the axis. Now, within a critical volume of radius r_c, any portion of a flux line experiencing a fluctuation into a left-handed helix is unstable and driven to expand radially out of the wire. One may now visualize a lattice of coexisting cylindrical sheets of helical flux lines, some right-handed and some left-handed. The right-handed migrate radially inwards, the left-handed migrate radially outwards. The two sublattices cut through each other continuously. We note that in this scheme both the ingoing and the outgoing helical flux lines contribute to the flux flow electric field $\vec{E} = -v(r)B(r)\hat{z}$. In chapter 4 we present observations which provide direct and unambiguous evidence that cylindrical sheets of helical flux lines can indeed be made to traverse each other.

1.3 Choice of Geometry and Procedure

As indicated above, the essential requirement for inducing flux cutting is that the component of the electric current $j_{||}$, flowing parallel to the flux lines exceeds the critical value $j_{c||}$. It is not necessary however that the total current I exceeds I_c. Further, it is frequently more convenient and sometimes advantageous to induce the persistent currents in the sample by Faraday induction, i. e. by changing the direction and also, if desired, the strength of an externally applied field. Both, the "direct feed" and the "induction" approach have been exploited in our laboratory

in the investigation of this phenomenon.

First, it may be useful to enumerate and describe the various arrangements which have been used to date in the study of flux cutting. We have already mentioned the choice of a long straight wire or ribbon immersed in a stationary longitudinal magnetic field $H_{||}$ and carrying a current I fed into the specimen through leads connected to an external current source. When the static current I exceeds I_c complementary data on the flux configuration and the dynamical steady state flux cutting can be obtained simultaneously in two ways. The flux flow voltage measured with the voltage probes provides information on the steady migration of the azimuthal (or transverse) component of the magnetic flux. A pickup coil embracing the wire or ribbon monitors $\langle B_{||} \rangle$, the magnetic flux density in the sample along the static applied magnetic field $H_{||}$ and the evolution of $\langle B_{||} \rangle$ when I is made to change.

In our laboratory, besides making extensive use of this setup, we have pioneered the development of methods where the supercurrent is induced to flow with component along the flux lines and thereby causing flux cutting to occur. A straight segment of ribbon is a convenient geometry, both from the aspect of sample preparation and analysis of the behaviour. The ribbon is first permeated by a homogeneous lattice of straight and parallel flux lines by allowing it to become superconducting in a uniform magnetic field directed along its length. This steady magnetic field, denoted $H_{||}$ (parallel to the axis of the cylinder), is readily provided by a superconducting solenoid. Persistent currents are now induced to flow along the flux lines by applying a magnetic field, denoted $H_{\perp}$, which is directed transverse to $H_{||}$ and along the flat faces of the ribbon. By the Faraday - Lenz law of electromagnetic

induction currents will be induced to circulate along and around the body of the ribbon to oppose any change in the magnetic flux threading it. These induced currents are persistent since the material is superconducting. As $\Delta H_\perp$, the change in $H_\perp$ progresses, the volume occupied by the currents expands because the local current density j cannot exceed its critical value $j_c(B,T)$ characteristic of the given material. Eventually saturation is reached where the entire cross section of the sample is occupied by the currents. Information on the macroscopic effect of flux transport and flux cutting processes which take place is gleaned by embracing the ribbon with two orthogonal pickup coils, one monitoring $\langle B_\perp \rangle$ and the other $\langle B_\parallel \rangle$, the components of the magnetic flux density along $H_\perp$ and $H_\parallel$ respectively. The signals from these detectors are integrated, amplified and recorded continuously and simultaneously as $H_\perp$ is varied at any desired rate. Hence, the evolution of the flux configuration as flux cutting and flux migration take place can be observed over various ranges of flux densities. We note that as the rise in $H_\parallel$ progresses, a change occurs in the angle β_s subtended between the total externally applied magnetic field, $\vec{H}_s = \hat{y}H_\perp + \hat{z}H_\parallel$ and its increment, $\Delta\vec{H}_s = \hat{y}\Delta H_\perp + \hat{z}H_\parallel$ (see accompanying sketches on Figure 2). Consequently, any change $\Delta\vec{j}_s$ in the current density $\vec{j}_s$ induced by the application of an increment $\Delta H_\perp$ is expected to subtend an angle α_s with respect to $\vec{H}_s$ which will increase as the latter evolves. This finally leads to $\Delta j_{s\parallel}$, the component of Δj_s parallel to $\vec{H}_s$, becoming progressively less dominant and eventually falling below the threshold for flux cutting to occur. In order to minimize this possibility and maintain the situation where the induced current at the surface is predominantly generated parallel to the existing (instantaneous) external $\vec{H}_s$ we can proceed as follows. $\vec{H}_s$ is rotated while its magnitude is kept

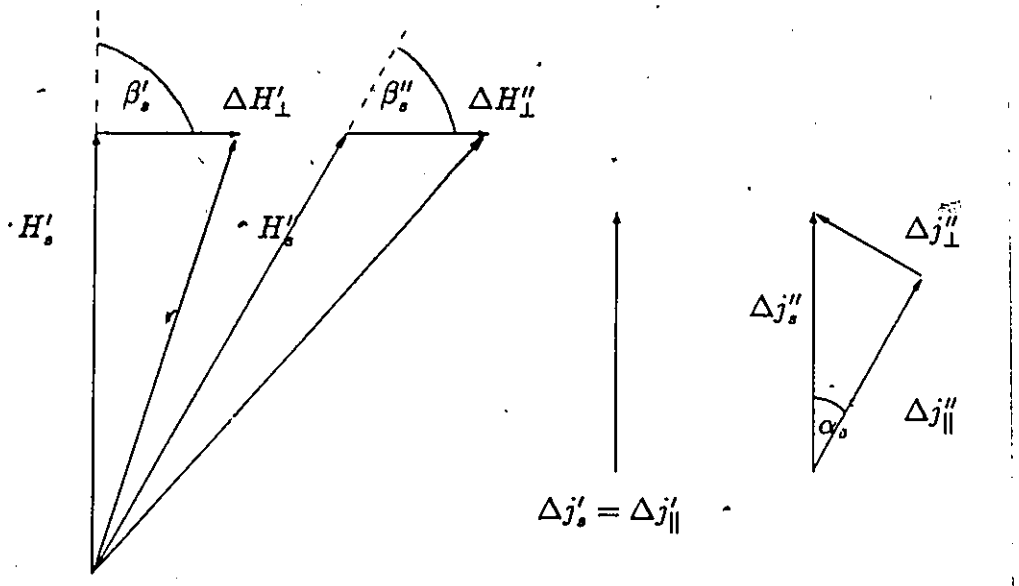

Figure 2: Two subsequent configurations of externally applied fields $\vec{H}_\parallel$ and $\vec{H}_\perp$ and resulting currents induced by the change $\Delta\vec{H}_\perp$

fixed (see Figure 3). Alternatively and equivalently, H_s is kept fixed in strength and in direction while the specimen is rotated with its flat surfaces along $\vec{H}_s$. In our laboratory we have focused on the latter approach and investigated flux cutting phenomena in disks of type II superconductors made to rotate (or oscillate) slowly or incrementally in a stationary, externally applied field $\vec{H}_s$, provided by a superconducting solenoid. Figure 3 schematically displays the situation where $\vec{H}_s$ rotates at constant magnitude ($\mid \vec{H}_{1,s} \mid = \mid \vec{H}_{2,s} \mid$). By the law of induction, Δj_s is generated orthogonally to $\Delta\vec{H}$, hence always parallel to $\vec{H}_s$.

For both disk and ribbon samples although the ratio of the thickness to diameter (or to length and width) can be made small to ensure that the demagnetization factor in the direction of the externally applied field $\vec{H}_s$ (always parallel to the broad surfaces) is not appreciable, various observations indicate that edge or end effects can play significant roles in the measurements. Motivated, in part, by the desire

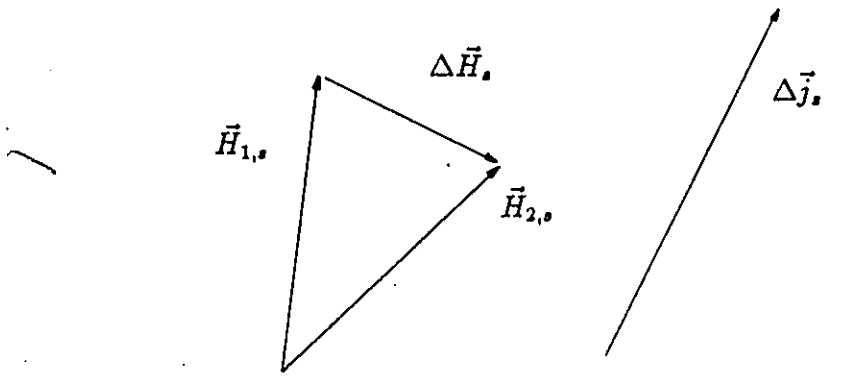

Figure 3: Rotating external magnetic field $\vec{H}_a$ and resultant induced currents $\Delta\vec{j}_a$ parallel to the field

to reduce this annoying feature, we have turned to long hollow cylinder geometry where the demagnetization factor along the azimuthal direction vanishes.

In terms of the spatial coordinates and taking the finite nature of the specimen into account, the configuration of the magnetic flux density can be written:

$$\vec{B}(x,y,z) = \hat{x}B_x(x,y,z) + \hat{y}B_y(x,y,z) + \hat{z}B_z(x,y,z) \tag{2}$$

for the ribbon and disk geometry, and:

$$\vec{B}(r,z) = \hat{r}B_r(r,z) + \hat{\phi}B_\phi(r,z) + \hat{z}B_z(r,z) \tag{3}$$

for the hollow cylinder geometry. Similar expressions can be written for the other pertinent physical quantities, the current density $\vec{j}$ and the electric field $\vec{E}$ generated by changes in $\vec{B}$.

Assuming infinite slab and infinite hollow cylinder geometry, the mathematical descriptions simplify considerably in both situations but the advantage or merit of the hollow cylinder now "disappears" in the formulation:

$$\vec{B}(x) = \hat{y}B_y(x) + \hat{z}B_z(x)$$

$$\vec{B}(r) = \hat{\phi} B_\phi(r) + \hat{z} B_z(r)$$

for the plane and cylindrical geometry respectively.

Generally, two regimes of behaviour need to be explored, namely the rate dependent and the rate independent regimes. Mathematically these two situations can be expressed as follows for the idealized cylindrical geometry under consideration:

$$\vec{B} = \vec{B}(r, H_s(t), \frac{dH_s}{dt})$$

for the rate dependent case, and

$$\vec{B} = \vec{B}(r, H_s)$$

for the rate independent case, with analogous statements for $\vec{j}$ and $\vec{E}$. The crucial distinguishing feature is that in the latter case the sequences of configurations of $\vec{B}(r)$, $\vec{j}(r)$ and $\vec{E}(r)$ which are encountered are controlled solely by the history of the externally applied field $\vec{H}_s$ when the sample is in the superconducting state and are not affected by the specific choice of the functional form for $H_s(t)$ and the duration of time taken to implement the changes.

In this initial phase of our investigation of flux cutting we have focused on the rate independent ("zero frequency") regime since, in our view, a good understanding of the phenomena under these circumstances will be required in order to unravel the more complicated behaviour expected when time dependent effects come into play.

Hollow cylinder geometry provides a remarkable and unique "laboratory" for the study of flux cutting aside from the feature that here the demagnetization factor along the azimuthal direction is zero. The longitudinal magnetic flux embraced by

the continuously connected cylindrical wall is, in a sense, a "conserved quantity". The "level" of flux cutting in this reservoir can only be changed by transfer to and from the enclosing wall and via the wall to and from the outside world. Once the hollow cylinder is in the superconducting state, the longitudinal flux density in the cavity, B_{zh}, is no longer dictated by the experimentalist but ensues from processes occurring in the wall under the action of the varying applied field. Consequently, B_{zh} becomes a property of the material. The important feature is that this quantity can readily be measured. Further, B_{zh} is a boundary condition for the sample, although it is beyond the control of the investigator. Models devised to account for the phenomena under scrutiny must therefore "predict" the evolution of this boundary condition as well as the observations of the changes in the spatial average of the components of magnetic flux permeating the wall. Because of this "decoupling" or "emancipation" of B_{zh}, measurements of flux cutting with hollow geometry presents a more severe test and formidable challenge to theory than data obtained with the other arrangements exploited in these studies.

Chapter 2

2.1 Choice of Sample

The general concept that flux lines in type II superconductors can and must undergo flux cutting processes when a large current density is caused to flow along the flux line lattice is now probably a universally accepted idea by workers in the field. It may be remarked however, that most workers in superconductivity are not aware of this concept. One reason for this is that the concept was developed after most of the books on superconductivity were published. Also the development of this concept and the exploration of its consequences and manifestations is still in its infancy.

Further, the relationship of this process to other aspects of the behaviour of type II superconductors is still a total mystery. For instance, it is well established that the surface of type II superconductors can act as a powerful barrier against the entry and the exit of magnetic flux. An understanding of the physics of this barrier, its origin and nature, continues to elude workers in this area. It is perhaps not surprising then that our knowledge of flux cutting at the surface barrier is non existent.

The density of flux lines, $\vec{B}$, in the bulk of isotropic type II superconductors is usually regarded as existing in equilibrium with a local thermodynamic magnetic field $\vec{H}$ regardless of previous history and whether pinning sites are present or not. This condition is denoted intrinsic equilibrium or Abrikosov diamagnetism in the literature and written $B_{eq}(H)$ or $H_{eq}(B)$. The theoretical studies of flux cutting published to date have however ignored this basic feature and all assume $\vec{B} = \mu_0 \vec{H}$. Thus reversible behaviour and Meissner flux expulsion currents have not been incorporated into the framework of flux cutting even in a phenomenological context.

Finally, the important and basic question of the role of pinning sites in catalysing or impeding flux cutting processes has yet to be investigated.

For the experimental investigator, regardless of the state of the theoretical understanding, it is important that the numerous aspects of the problem be examined systematically, hence separately and sequentially. The experimental program can easily be mapped out and divided into several compartments:

- Exploration of flux cutting phenomena in the bulk of a type II superconductor in situations where flux pinning is dominant, hence where surface barrier effects are absent or negligible and intrinsic diamagnetism can be ignored. Thus the sample should be very hysteretic in its classical (flux transport) magnetization curve but display no or small surface pinning in its magnetic response.

- Examination of flux cutting in a very reversible (nearly ideal) type II superconductor, i. e. a specimen essentially free of pinning and with no surface

barrier.

- Study of flux cutting on a sample where the surface barrier is large, the bulk devoid of pinning and H_{c1} small compared to H_{c2}, hence intrinsic diamagnetism negligible when $H_{c1} < H_s < H_{c2}$.
- Finally, the investigation of flux cutting behaviour in a sample where the surface barrier, bulk pinning and reversible currents all play comparable roles can then be envisaged.

Among the several materials which meet the requirements listed above, the Pb rich PbBi alloys, in particular the eutectic $Pb_{0.45}Bi_{0.55}$ offers many advantages. Firstly, the superconducting transition temperature is about 6.3 K, hence flux cutting phenomena can be conveniently studied at 4.2 K, the temperature of liquid helium at atmospheric pressure. This considerably simplifies the experimental environment. Since at 4.2 K, the lower critical field $H_{c1} \approx 50$ mT, and the upper critical field $H_{c2} \approx 1.5$ T, the vortex state spans a very broad range of flux density with an upper limit which is not excessively large and can be attained with the small, inexpensive superconducting coils fabricated in our laboratory. As a consequence, we can scan the effect of flux line density on flux cutting processes with some ease. In our sample, the criterion that flux pinning dominate intrinsic diamagnetism is well satisfied both at low fields ($H \leq H_{c1}$) and in the vortex state between H_{c1} and H_{c2}. At low fields this can be seen from the observation that the residual trapped flux density is comparable to $\mu_0 H_{c1}$. In the vortex state this emerges from the fact that the ascending and descending magnetization curves are nearly symmetric. Inspection of minor hysteresis loops shows no evidence of

surface barriers to flux entry and exit. It is also well established that annealing the quenched eutectic can appreciably modify the pinning strength and transform the sample from a highly irreversible to a semi-reversible type II superconductor.

From the viewpoint of sample preparation this material is most appealing indeed. The constituents in very pure form are inexpensive. Finally, because of the low melting temperature of the components and of the alloy, it is a straightforward matter to prepare a massive, homogeneous ingot from which the hollow cylinder can be machined.

2.2 Sample Preparation and Specifications

The hollow cylindrical $Pb_{0.45}Bi_{0.55}$ sample is 100 mm in length, 3.45 mm of inner radius and 4.15 mm of outer radius. The ingot was prepared by melting the high purity components at the eutectic proportions in an evacuated glass tube at the temperature $T \approx 600°$ C. After several hours in this temperature during which time the glass tube was repeatedly shaken, the alloy was quenched by abruptly moving the glass tube from the furnace into the room. The hollow cylinder was formed from this cylindrical ingot by machining on a lathe and drilling the hole. The sample was not subjected to any further mechanical or chemical treatment. The sample was prepared by Fillion [17] and investigated as part of his research for his PhD thesis.

2.3 Experimental Set-up

2.3.1 The Sample - Heater Assembly

It is important in the study of the magnetic and critical current behaviour of type II superconductors that the initial configuration of the magnetic flux for each measurement be known and controlled. Consequently, in a sequence of measurements, the previous magnetic field history of the specimen in the superconducting state needs to be erased and a fresh start from a chosen "virgin" state can be made. This is accomplished by raising the temperature of the sample above its transition temperature T_c and allowing it to cool from T_c to 4.2 K (or some other chosen operating temperature) in the desired initial, externally applied magnetic field $H_{\parallel}$ and/or H_{ϕ}.

A formvar insulated manganin heater wire was wound directly around the external circumference of the sample over its entire length as shown on Figure 4. This single layer heater is wound very tightly to ensure uniformity of the winding, hence of the temperature distribution. A bifilar noninductive arrangement is used where adjacent turns of the heater carry current flowing in opposite directions, hence no net magnetic field is generated when the heater is made to carry a current. Manganin is used because its resistivity is large and nearly temperature independent over the range from absolute zero to room temperature. Further, this alloy is non-magnetic, hence contributes no background signal to the measurement.

The sample-heater system is inserted into a well fitted thin perforated delrin sleeve. The perforations allow evaporating helium to escape. The sleeve provides a smooth surface on which the pickup coil can be wound and also acts as a frame for

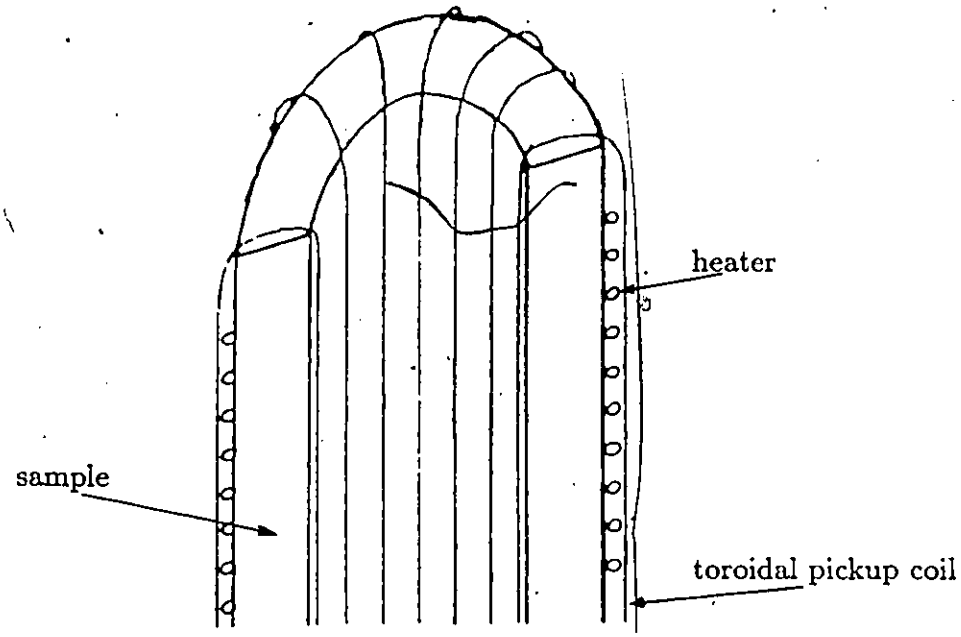

Figure 4: A cross section through the sample - heater assembly

fixing and holding the sample in place inside the magnet coil assembly.

2.3.2 The H_z and H_ϕ magnets

The axial magnetic field H_z is produced by a superconducting solenoid, 17.6 cm long, with an inner radius of 1.9 cm and outer radius of 4.9 cm. This solenoid is made appreciably longer than the hollow cylinder sample (10 cm) so that the latter bathes in an axial field homogeneous to $\leq 2\%$ over its volume. The superconducting magnet was made in our laboratory using 0.4 mm diameter formvar insulated, multifilamentary NbTi wire (Supercon). The magnet is energized using a transistorized, battery driven power supply designed and built in the physics electronics shop and provides 0.0716 Tesla/Ampere.

The generation of a sufficiently strong azimuthal magnetic field H_ϕ presents a formidable challenge. The criterion for a sufficiently strong H_ϕ is that starting from $H_\phi = 0$ with the sample in a flux free state, the cycle of H_ϕ should generate the maximum residual trapped flux configuration. For our sample this means that $\mu_0 H_\phi$ should exceed 0.12 Tesla. We stress however that this constitutes a minimum requirement and it is highly desirable to significantly surpass this threshold value. Fillion [17] for his investigations on this sample had developed a configuration which just attained this objective. We redesigned and rebuilt the toroidal magnet coil arrangement and achieved $H_{\phi max} \approx 0.3$ Tesla. As will be seen in chapter 4 of this thesis, this enhanced performance enabled us to observe fascinating behaviour which is not encountered in the range of fields available to Fillion. We refer the reader to Figure 5 which shows schematically the toroidal magnet and the inner pickup coil system.

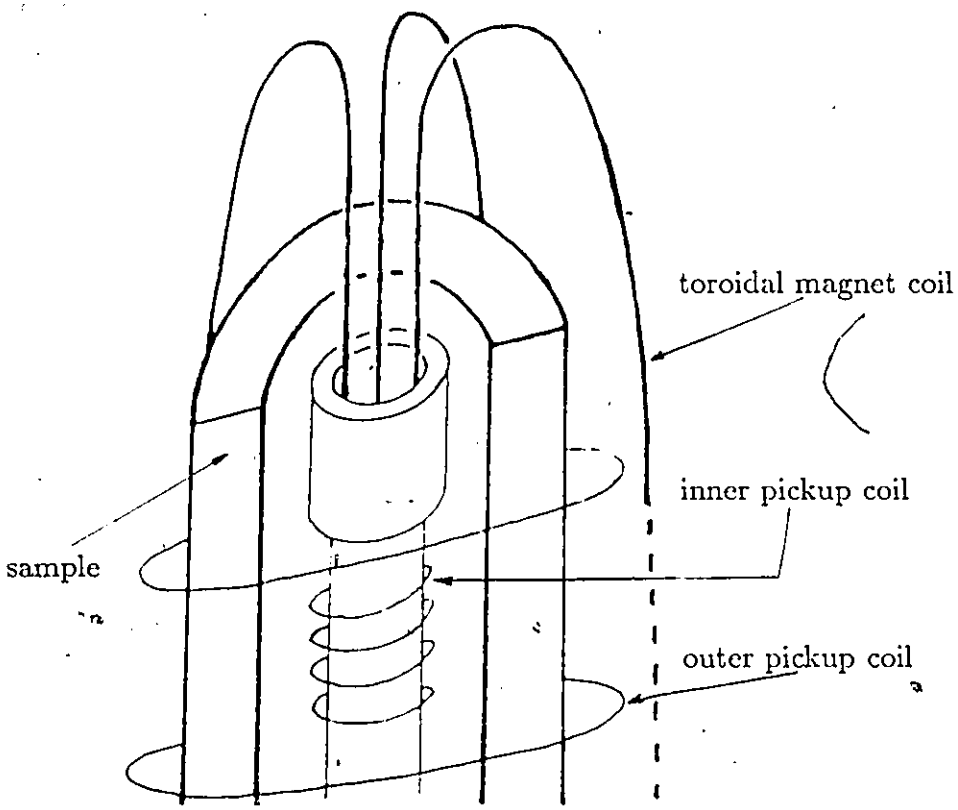

Figure 5: A cross section through the sample with inner pickup coil and azimuthal magnet coil

H_ϕ is provided by causing a steady current I to flow in the toroidal coil wound around the wall of the hollow cylinder as shown in Figure 5. The turns of this toroidal coil must thread through the cavity of the hollow cylinder and share the available cross section of this hole with the windings of the toroidal pickup coil and an axial pickup coil. The largest direct current supply in our laboratory can provide a maximum of 400 Amperes. Superconducting NbTi wire was selected, which can safely sustain current of this magnitude at 4.2 K, in an ambient magnetic induction of about 1.5 Tesla (the axial magnetic field H_z) and in the presence of heat flow from the adjacent heater. Further, this wire must undergo sharp bending when wound into a toroidal coil. Hence, multifilamentary twisted NbTi wire embedded in a copper matrix was used. Since the inner loops of the toroidal pickup coil should be placed snugly against the inner wall of the hollow cylinder and the axial pickup coil should embrace as large an area as possible, it is evident that the winding of the toroidal magnet coil must pass through a hole at the centre along the axis of the inner pickup coil. In our arrangement we managed to wind a coil of 16 turns (as compared with 7 for Fillion). At the same time we succeeded in increasing the average area-turn product of the inner pickup coil by a factor of two, hence increasing its sensitivity by this amount. This was achieved by using much finer copper wire (48 B&S) for this coil and fitting it more tightly into the available space.

We wish to send as much as 400 Amperes of direct current for time intervals of several minutes duration in the toroidal coil. This large current is close to the critical value for this wire at the ambient temperature of 4.2 K. Consequently, the contact resistance between the copper leads and the superconducting wire must be minimized (contact resistance no higher than a microohm is desirable). Further, the

unavoidable Joule heat at the copper-superconductor interface must be efficiently removed by conduction to the liquid helium bath. We reduce the contact resistance by providing for good electrical contact to several centimeters of the ends of the superconducting wire and at the same time we provide for rapid heat dissipation as follows. At the "contact" the copper wire leads are attached to massive copper blocks. These are then screwed tightly together compressing a thin sheath of indium which embraces the ends of the superconducting NbTi wire. The indium intimately wets both the surface of the NbTi wire and the adjacent surfaces of the copper blocks. The latter serve as reservoirs for the Joule heat and at the same time distribute this heat to a large volume of the liquid helium.

In the event that the critical current of the superconducting toroidal coil is exceeded, an electronic relay rapidly (in a time shorter than 5 milliseconds) interrupts the current by turning off the driving voltage inside the transistorized power supply. This protects the toroidal coil from damage by local heating along any section transiting from the superconducting to the normal state (the copper sheath surrounding the NbTi core provides only short term protection at these large currents). The electronic relay is activated when a voltage of a few millivolts appears across the toroidal magnet coil.

We stress that the azimuthal magnetic flux density B_ϕ along the inner surface of the hollow cylinder is greater than that at the outer surface by a factor of 1.2 since $B_\phi(R_i)/B_\phi(R_o) = R_o/R_i = 1.2$ for our sample.

Using Ampere's law, the applied azimuthal magnetic field is given by:

$$H_\phi(r) = \frac{nI}{2\pi r}$$

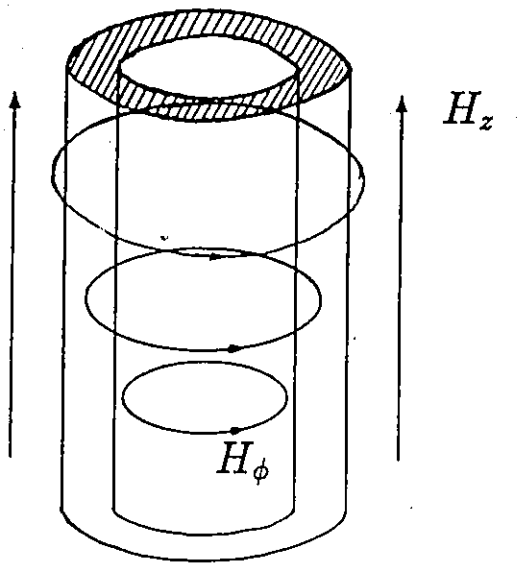

Figure 6: The sample subjected to the combination of axial magnetic field H_z and azimuthal magnetic field $H_\phi(r)$.

where n is the number of turns of the toroidal magnet coil ($n = 16$ in our setup). The average azimuthal magnetic induction permeating the wall of the cylinder in the normal state can be written as :

$$\langle B_\phi \rangle_{applied} = \frac{\int B_\phi(r) dr}{\int dr}$$

or after integration:

$$\langle B_\phi \rangle_{applied} = \frac{\mu_0 n I}{2\pi(R_o - R_i)} \ln \frac{R_o}{R_i} \tag{4}$$

where R_o and R_i are the outer and inner radii respectively. Figure 6 shows the combination of magnetic fields bathing the sample during our measurements. In the work reported in this thesis we induce flux cutting by varying (increasing or decreasing) H_ϕ while maintaining $H_\parallel$ fixed.

2.3.3 The Monitoring System

We obtain information on flux transport and the occurrence of flux cutting processes in the sample by (i) continuously monitoring the evolution of the axial magnetic flux density threading the cavity of the hollow cylinder and (ii) monitoring the configuration of magnetic flux permeating the wall as (iii) the boundary conditions $H_\phi(R_i)$, $H_\phi(R_o)$ and $H_z(R_o)$ are made to vary according to some chosen prescription.

The longitudinal magnetic flux density in the hole, B_{zh}, is monitored using an "inner" pickup coil positioned centrally along the axis of the cavity. This pickup coil comprises about 26,000 turns of 48 gauge formvar insulated copper wire. The windings occupy a cylindrical volume of 64 mm length, 2.72 mm inner radius and 3.75 mm outer radius. We stress that the length of this coil is deliberately chosen much smaller than that of the hollow cylinder sample (100 mm), so that the axial magnetic flux density it monitors corresponds to that threading the "waist" of the cavity of the specimen and does not include end effects. This pickup coil is more sensitive than that used by Fillion [17] by a factor of about 2.

In some measurements it is convenient to monitor $\Delta H_z = H_{||} - H_{zh}$, the difference between the axial externally applied field and the axial field in the hole. This is particularly useful when $H_{||}$ is being varied over a wide range. For these measurements we have positioned an axial bucking coil outside the sample but inside the solenoid with an average area-turn product corresponding closely to that of the inner axial coil. With these two coils connected in series opposition the evolution of ΔH_z as $H_{||}$ is swept up or down can be traced directly.

The azimuthal magnetic flux density permeating the wall, $\langle B_\phi \rangle$, is monitored

with a toroidal pickup coil embracing the latter. This coil contains some 2000 turns of 48 B&S copper wire distributed among 5 layers wound directly and manually along the wall and through the cavity using a shuttle. It surrounds the wall, the heater and the thin delrin sleeve. An 8100 turns (42 B&S) bucking coil of small area is positioned just outside one end of the hollow cylindrical sample but inside the toroidal magnet coil. This pickup coil senses the applied azimuthal magnetic induction $\langle B_\phi \rangle_{app}$. Its area-turn product matches closely that of the toroidal pickup coil embracing the wall. Consequently, with these two coils connected in series opposition we can continuously and directly monitor $\Delta\langle B_\phi \rangle = \langle B_\phi \rangle - \langle B_\phi \rangle_{app}$, the difference between the azimuthal flux permeating the wall and the applied azimuthal flux. It is this difference which contains the desired information.

The longitudinal magnetic flux threading the sample is monitored with a large pickup coil embracing the "waist" of the hollow cylinder. This coil is 57 mm long, with an inner radius of 9.5 mm and an outer radius of 16 mm. It is positioned symmetrically around the centre of the sample and is constructed shorter than the latter to avoid measuring any distortions of the magnetic flux due to edge effects. This coil actually consists of two concentric oppositely wound, series connected pickup coils where, $N_o\langle A_o \rangle$, the turn-area product of the outer coil, matches $N_i\langle A_i \rangle$, the turn-area product of the inner coil. It contains some 180,000 turns, ($N_o + N_i$), of which some 60,000, ($N_i - N_o$) provide the resultant signal. This scheme was exploited because it allows us to use a much shorter solenoid than would be required in the alternative approach where the balancing coil is positioned away from the sample but inside the solenoid.

Since this pickup coil is balanced, it is (ideally) insensitive to changes in the

axially applied magnetic flux density $\mu_0 H_{\|}$ and only registers changes in the net flux threading the sample. This can be written,

$$\Delta\Phi_z = \Phi_z - \mu_0 H_{\|} A_s$$

where $A_s = \pi R_0^2$ is the cross section of the hollow cylinder and R_0 its outer radius. From the perspective of this pickup coil, the hole is an integral part of the "sample". Consequently, changes in the axial flux threading the hole as well as the wall will be detected by this pickup coil. Any transfers and exchanges of axial flux between the cavity and the wall will however generate no signal in this detector. Such events will however be recorded by the inner axial pickup coil.

The output signal from each pickup coil pair (driving and bucking coil) feeds an integrator-amplifier (PAR model 215) which then drives one of the axes of an X-Y recorder. The other axis of the recorder is driven by a signal proportional to the applied magnetic field which is being varied. This signal is generated by the voltage drop $V_R = IR_s$, appearing along a shunt of resistance R_s, placed in the circuit of the toroidal magnet coil.

2.4 Measurement Procedure.

2.4.1 Calibration

The persistent shielding current induced to flow in a superconducting specimen in the "virgin" state by the application of a weak magnetic field (H_ϕ or $H_{\|}$) is assumed to flow entirely in λ, the penetration depth at the surface of the hollow

cylinder. "Virgin" state here means that the sample has been allowed to cool from $T \geq T_c$ to 4.2 K in zero applied field. Since $\lambda \approx 1000$ Angstrom is minute compared to any of the dimensions of the sample, the response of the sample to a weak applied magnetic field ($H < H_{c1}$) is perfectly diamagnetic and linear. Thus the integrated signal S registered on the Y axis of the X-Y recorder is proportional to the applied field H driving the X axis, hence $S = kH$. The signal S contains however a linear contribution which is extraneous since generally the pickup coils are not perfectly balanced. We can now distinguish and determine the true and extraneous contributions to S by driving the sample into the normal state by raising its temperature to T_c with the heater while maintaining H fixed.

2.4.2 Background or Normal State Reference Curves

The use of superconducting magnet coils to generate magnetic fields imposes a price or penalty which is frequently not mentioned in the published papers. The relationship between H generated by the superconducting coil and the current I flowing in the latter is not exactly linear. Furthermore, and more troublesome, is the fact that H is not a single valued function but is a history dependent function of I. As a consequence, for each measurement, the selected history must first be "established" by taking the superconducting magnet coil(s) through the chosen sequence or cycle. Subsequently, for the chosen measurement procedure, the deviation of $H(I)$ from linear, hence single valued behaviour, must be determined by recording the reference curve with the sample absent (i. e. in the normal state). Finally, the observations with the specimen in the superconducting state are made and recorded.

The reason $H(I)$ is not single valued and is history dependent (hysteretic) for

superconducting magnet coils is that the winding not only carries the energizing current I but also supports complicated configurations of persistent currents induced by the changes in the H which the coil produces.

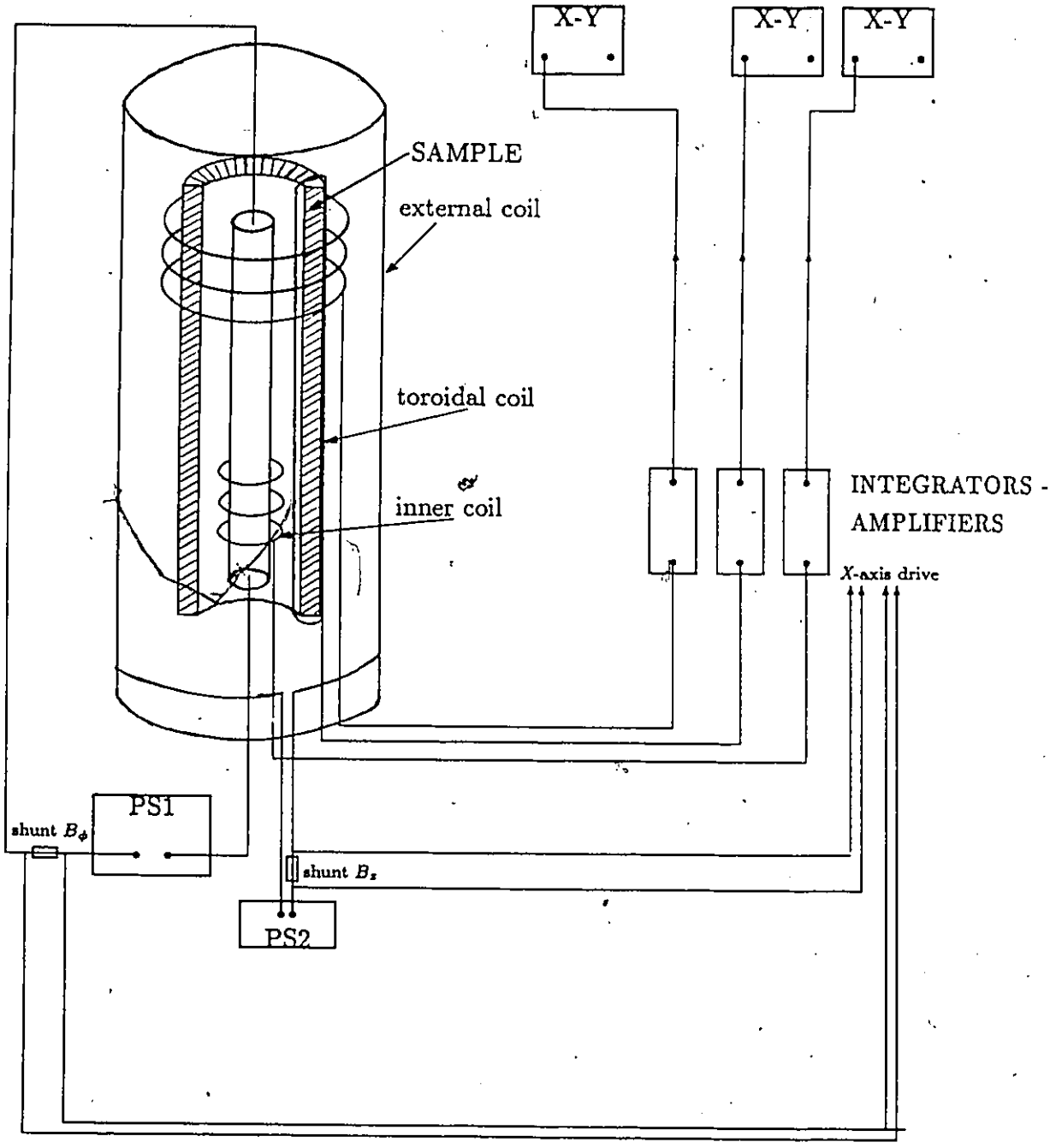

Figure 7: Complete scheme of the apparatus used for the measurements.

Chapter 3

3.1 The "Classical" Critical State Model

Before we present our experimental results and discuss their interpretation it may be useful to review and outline the pertinent physical framework which guided and motivated our research project.

It is now well established that in type II superconductors magnetic flux exists in the form of discrete flux lines each containing a quantum of flux $\phi_0 = h/2e$. In an ideal (pinning free) superconductor which has become superconducting in a static magnetic field $H_{c1} < H < H_{c2}$, the density of flux lines is uniform ($N(x) = B(x)/\phi_0$) and no net currents are flowing in the volume of the specimen. The material however is filled with electric currents. The axis of each flux line (flux vortex) is surrounded by an intricate "whirlpool" of persistent electric currents and a reversible screening (often referred to as Meissner or diamagnetic) current flows at the surface of the sample.

If now the externally applied field H_s is increased, new flux lines nucleate at the surface and migrate into the interior of the sample until a uniform density

distribution is established. Electrodynamic viscous drag governs the time required for the new equilibrium density to be achieved. The Abrikosov equilibrium flux line density $B_{eq}(H)$ is determined by the strength of the mutual repulsion between the flux lines and the repulsive interaction between the flux line lattice and the applied magnetic field existing in the penetration depth. When H_s is decreased, the mutual repulsion causes flux lines at the surface to be expelled and flux lines in the bulk to migrate towards the surface until the equilibrium density (Abrikosov equilibrium) is attained.

Pinning sites in the bulk of non ideal materials will oppose and impede the displacement of the flux lines. An individual flux line will be in a critical static state on the verge of moving when the net repulsive force it experiences is equal to the pinning force acting on it. A net repulsive force will arise when the flux line is surrounded by an asymmetric or nonuniform distribution of flux lines. In the context of Maxwell's equations, this state of affairs can be written, $\nabla \times \vec{B} = \mu_0 \vec{j}_c$ where $\mid \vec{B} \mid$ is regarded as an average over the cross section of several flux lines. For infinite slab geometry, this means that the gradient in the local density of flux lines, dB/dx, is in a critical state and a net current, $j_\perp$, flows transverse to the flux line at a critical density $j_{c\perp}$. This net current density, associated with the gradient in the flux line density by Maxwell's equation, arises from the superposition of the patterns of persistent currents circulating around the axis of each flux line. This superposition now yields a net current density since the flux line lattice is no longer uniform.

For simplicity we continue to focus on straight, parallel arrays of flux lines. Several authors have shown that the net repulsive force acting on a unit length of

a flux line situated in a nonuniform flux line lattice, is given by $j_\perp \phi_0$ where $j_\perp$ is the current density generated at the axis of a flux line by the superposition of the patterns of the vortex currents of the neighbouring flux lines. This "driving" force has the form of the Lorentz force and can be conveniently written $\vec{F}_L = \vec{j} \times \vec{B}$, where $\vec{F}_L$ is a force density averaged over a volume occupied by several flux lines. The critical state concept envisages that the minimum driving Lorentz force which can appear in a type II superconductor under isothermal changes of flux line density must equal the local pinning force density $\vec{F}_p(B)$. This principle is expressed by the statement

$$\vec{F}_L = -\vec{F}_p.$$

Stated differently but equivalently, the critical state idea asserts that no changes in flux configuration can occur via flux transport, and hence no electric field $E_\perp$ can arise via flux displacement in type II superconductors unless $j_\perp > j_{c\perp}$ where $j_\perp$ is the current density flowing transverse to the flux line density $\vec{B}(x)$. Here $E_\perp$ is the electric field perpendicular to the axis of the flux lines.

For simplicity, we consider an infinite slab of a nonideal type II superconductor which has become superconducting in a homogeneous magnetic field H_s directed parallel to the surfaces of the slab of thickness X. Again an increase in H_s nucleates flux lines at the surfaces. Now however, because of pinning in the volume of the slab (bulk pinning) the migration of the flux lines into the slab is impeded and takes place only when the gradient of the flux line density $dB/dx \geq (dB/dx)_c$ or equivalently, $j_\perp \geq j_{c\perp}$. If the variation of H_s is not too rapid, the electrodynamic viscous drag is not important and the sequence of $B(x)$ profiles which is generated by the sweep of H_s does not deviate markedly from the critical configurations. At

any rate, when the change in H_s ceases, the flux line distribution will relax to a critical configuration. As the migration of the flux lines takes place under the action of the "Lorentz" driving force overcoming the pinning force, an electric field $E_\perp(x)$ is generated perpendicular to the axis of the flux line and to its velocity, $\vec{E} = \vec{v} \times \vec{B}$. This is often denoted the flux flow electric field since

$$V = -\int \vec{E} \cdot d\vec{r}$$

is the flux flow voltage. The migration (transport) of the flux lines dissipates energy at a rate $dP/dt = E_\perp j_\perp$. This must be provided by the source of the electric current (the source of the external magnetic field). The relationship, $\vec{E} = -\vec{v} \times \vec{B}$ is a formulation of the Maxwell-Faraday equation, $\nabla \times \vec{E} = -\partial \vec{B}/\partial t$ which explicitly expresses the picture of moving flux entities.

For hollow cylinder geometry, two situations need to be envisaged:

- $\vec{H}_s$ is directed along the axis of the cylinder ($\vec{H}_s = \hat{z} H_s$), or
- $\vec{H}_s$ is directed azimuthally ($\vec{H}_s = \hat{\phi} H_s$).

Introducing the classical critical state concept in Maxwell's equations

$$\nabla \times \vec{B} = \mu_0 \vec{j}$$

and

$$\nabla \times \vec{E} = -\frac{\partial \vec{B}}{\partial t}$$

we then obtain for an infinite cylinder geometry:

$$\frac{dB_z(r)}{dr} = -\mu_0 j_{c\perp}(r)$$

$$\frac{dE_\perp(r)}{dr} + \frac{E_\perp(r)}{r} = -\frac{dB_z(r)}{dt} \tag{5}$$

where $j_{c\perp} = j_\phi$, $E_\perp = E_\phi$, when $\vec{H}_s = \hat{z}H_s$ and:

$$\frac{dB_\phi(r)}{dr} + \frac{B_\phi(r)}{r} = -\mu_0 j_{c\perp}(r)$$

$$\frac{dE_\perp(r)}{dr} = -\frac{dB_\phi(r)}{dt} \tag{6}$$

where $j_{c\perp} = j_z$ and $E_\perp = E_z$ when $\vec{H}_s = \hat{\phi}H_s$. A crucial feature of the "classical" critical state concept is that $E_\perp = 0$ unless $j_\perp > j_{c\perp}$. The situation where $\vec{H}_s = \hat{z}H_s$ has been exploited to determine $j_{c\perp}$ versus B at various temperatures. The experimental approach is quite straightforward. The magnetic field, H_{zh}, in the hole of the cylinder is continuously monitored, with a pickup coil - amplifier - integrator system as in our work or some Hall effect probe, as the external field $H_\parallel$ is swept up or down. Clearly, when the entire cross section of the wall carries a critical current, Maxwell's equation reads:

$$H_\parallel - H_{zh} = I_c = \langle j_\perp \rangle (R_o - R_i) \tag{7}$$

The challenge in these endeavours is to determine $j_{c\perp}$ versus B and T for various materials from measurements of the magnetic response (for instance with the simple arrangement just described) or the critical current using current leads and a sensitive voltmeter (standard four probe technique). Conversely, starting with the knowledge of $j_c(B,T)$, the critical state idea incorporated in Maxwell's equation is exploited together with straightforward electrodynamic considerations to predict the magnetic behaviour and hysteresis (low frequency AC) losses for various geometries and circumstances.

In the terminology proposed by Clem and his collaborators, the regions where the flux density is changing are denoted T zones where the T stands for pure transport (transfer, migration or displacement) of flux. In the "classical" critical state framework, only two types of zones can exist:

- T zones where B is changing, $E_\perp \neq 0$ and $j_\perp \geq j_{c\perp}$
- O zones where B is static, $E_\perp = 0$ and $0 < j_\perp \leq j_{c\perp}$.

We stress that when $0 < j_\perp < j_{c\perp}$ occurs in a O zone, then at some earlier time, this zone existed as a T zone.

3.2 Non Parallel Flux Lines.

In the previous section we have considered only the standard and simple situation where the successive generations of flux lines created at the surface and migrating into the sample are directed parallel to each other and to that already permeating the material. This is sometimes referred to as a collinear configuration. We now envisage a slightly more complicated but nevertheless quite realistic scenario. For clarity it is convenient to first focus on a semi infinite half-space occupying the volume $x \geq 0$, initially permeated by a uniform lattice of straight parallel flux lines directed along the z axis. A homogeneous magnetic field $\vec{H}_\parallel = \hat{z}H_\parallel$ fills the empty space $x < 0$. Now we visualize that $\vec{H}_s$ is increased in magnitude while at the same time its direction is changed according to the prescription:

$$\vec{H}_s(t) = \hat{z}H_\parallel + \hat{y}H_y(t).$$

This particular evolution of $\vec{H}_s$ corresponds to that exploited in our experiments and is also conceptually straightforward. Let α_s denote the angle subtended at the surface of the superconductor between $\vec{H}_s$ and its $\vec{z}$ component, hence $\alpha_s(t) = \cos^{-1}(H_{||}/H_s(t))$. According to prevailing ideas, the successive generations of flux lines created at the surface of the superconductor because of the increase in $\mid H_s \mid$, and migrating into its volume will be directed at an angle $\alpha_s(t)$ which is increasing as $H_y(t)$ increases. Let us now assume that a uniform distribution of pinning sites exists in the superconducting material. As a consequence, a critical gradient in flux line density, $dB/dx = \mu_0 j_{c\perp}$, will develop in a volume adjacent to the surface, $0 < x < x_p$. Here x_p denotes the boundary of penetration of the flux compression or disturbance (the interface between the advancing T zone and the shrinking O zone).

Further, let us assume that the flux lines retain the orientation they possessed at the time of their creation while they migrate into the superconductor. Consequently, a gradient $d\alpha/dx$ will also develop in the configuration of the orientation of the flux lines. However, Maxwell's equation, $\nabla \times \vec{B} = \mu_0 \vec{j}$ for semi infinite slab geometry can be shown to read:

$$B\frac{d\alpha}{dx} = \mu_0 j_{||} \tag{8}$$

where $j_{||}$ denotes the current density flowing parallel to $\vec{B}(x)$, hence parallel to the direction of the flux lines.

Pursuing the concept of conservation of flux lines inside the superconducting material together with the concept that flux lines retain their initial orientation, we note that, as a consequence, the volume $0 \leq x < x_\alpha$ occupied by $j_{||}$ (or equivalently by the gradient of α) is smaller than the volume occupied by a current $j_{c\perp}$ (or

equivalently by the critical gradient of flux density), i. e. $x_\alpha < x_p$. At any time, therefore, the superconductor contains the following flux along the z direction:
(i) all of the flux initially permeating it, a portion of which is now compressed in the volume $x_\alpha < x < x_p$, and
(ii) the $\vec{z}$ component of the flux which has been nucleated since the growth in $\mid \vec{H}_s \mid$ commenced.

As a consequence, the component of the flux density along $H_\parallel$ is seen to rise as H_y is made to increase. Another way of seeing this important result is to note that every flux line introduced into the superconductor by the growth in $\mid \vec{H}_s \mid$ carries a unit of flux ϕ_0, hence adds an amount ϕ_0 of flux along the z axis. Considering now an infinite slab instead of an infinite half-space, we can see that as H_y increases, $\langle B_z \rangle$ must grow monotonically until $H_s = H_{c2}$.

Maxwell's equations, $\nabla \times \vec{B} = \mu_0 \vec{j}$ and $\nabla \times \vec{E} = -\partial B/\partial t$ can be written to incorporate these ideas as follows:

$$\frac{\partial B}{\partial x} = -\mu_0 j \geq \mu_0 j_{c\perp} \tag{9}$$

$$B\frac{\partial \alpha}{\partial x} = \mu_0 j_\parallel \tag{10}$$

$$\frac{\partial E_\perp}{\partial x} = -\frac{\partial B}{\partial t} \tag{11}$$

$$E_\perp \frac{\partial \alpha}{\partial x} = -B\frac{\partial \alpha}{\partial t} \tag{12}$$

for planar geometry, and:

$$\frac{\partial B}{\partial r} + \frac{B\sin^2\alpha}{r} = -\mu_0 j_\perp \geq \mu_0 j_{c\perp} \tag{13}$$

$$B\left(\frac{\partial \alpha}{\partial r} + \frac{\sin\alpha\cos\alpha}{r}\right) = \mu_0 j_\parallel \tag{14}$$

$$\frac{\partial E_\perp}{\partial r} + E_\perp \frac{\cos^2 \alpha}{r} = -\frac{\partial B}{\partial t} \tag{15}$$

$$E_\perp (\frac{\partial \alpha}{\partial r} - \frac{\sin \alpha \cos \alpha}{r}) = -B \frac{\partial \alpha}{\partial r} \tag{16}$$

for infinite cylinder geometry (solid or hollow), where α is the angle subtended by $\vec{B}(r)$ and the axis of the cylinder. Again we stress that $E_\perp = 0$ unless $j_\perp > j_{c\perp}$.

It quickly becomes evident as we observe the evolution of the magnetic flux in the wall of our hollow cylinder sample when $\vec{H}_s(t)$ is made to change as specified above that something is amiss. We see immediately that the magnetic flux density along the direction of the static component of $\vec{H}_s(t)$ does not increase monotonically. Indeed, quite frequently an initial and substantial diminution occurs in this quantity. We will see this in the next chapter. We are thus inexorably led to conclude that flux lines do not always retain their initial orientation as they are compressed and made to migrate.

3.3 The Generalized (Flux Cutting and Flux Pinning) Critical State

The magnetic flux density along the static component $\vec{H}_{||}$ of an applied magnetic field $\vec{H}_s$ varying in direction and increasing in strength is frequently observed to diminish although flux lines are being pumped into the specimen, each of which adds a quantum of flux along $\vec{H}_{||}$. It is often suggested that rotation of the flux lines in the sample, away from $\vec{H}_o$ and toward $\vec{H}_s$, can account for this phenomenon. This explanation however requires that some mechanism(s) exist which will cause the flux lines to rotate.

Driving (Lorentz like) forces tending to rotate flux lines indeed appear in a volume of depth λ around the two end points where a flux line pierces the surfaces of a specimen. These driving forces, however, must overcome the pinning forces anchoring the flux line along its entire length. Since the competing force densities are comparable, the ratio of the torque tending to rotate a flux line to that opposing the rotation is approximately $\lambda/l \approx 10^{-5}$. Processes which will lead to a change in the orientation of flux lines must consequently be sought in the interactions and behaviour of flux lines inside the body of the superconductor. Clem and his collaborators [10,11,12,15] and Brandt [1,2,3] have pursued this question in some detail. All these accounts visualize that flux lines cut and rejoin at points of intersection. We now outline the two complementary pictures developed by these workers.

The sequence of events is depicted in Figure 8. We visualize a lattice of flux lines consisting of sheets of parallel flux lines where the angle subtended by any adjacent pair of sheets is denoted Θ. For simplicity, we consider the linear density of flux lines in the sheets to be uniform. A configuration of flux density with the properties just described can exist only if sheets of uniform current density $\vec{j}(x)$ permeate the lattice with $\vec{j}$ directed along the flux lines. Thus Maxwell's equation $\nabla \times \vec{B} = \mu_0 \vec{j}$ is satisfied. Here $\vec{j}$ is regarded as a quasi microscopic average over cross sections less or equal to that of a flux line and denoted $j_{\|}$.

We now focus on a pair of adjacent sheets (see Figure 8/(a)). It was shown by Clem and Yeh [16] and Brandt et al. [3] that as the angle Θ, hence the current $j_{\|}$, are chosen larger and larger, the repulsive interaction between the sheets of flux lines diminishes and, at some critical value Θ_c (hence $j_{c\|}$) the interaction becomes one of mutual attraction. The two sheets can be viewed as driven towards each other

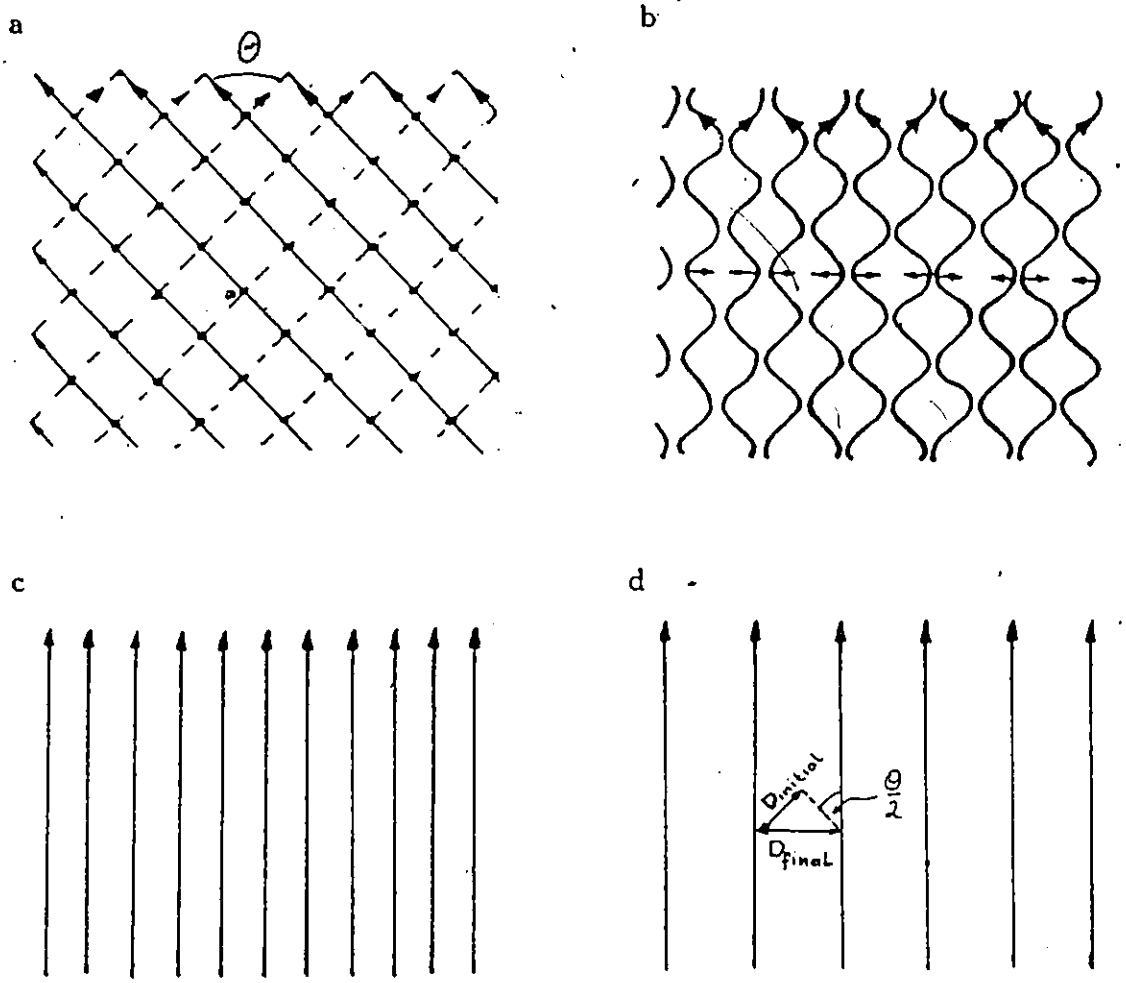

Figure 8: Two planes of vortices merging together (a), zigzag vortices created as doubly quantized vortices break into two singly flux lines (b), zigzag vortices straighten (c) and two planes of identical orientation move apart (d).

by a Lorentz like force $\vec{j} \times \vec{B}$ where $\vec{j}$ is a current density in the midplane between the two sheets. The two sheets are thus made to intersect and the adjacent ends of segments at the contact points to cross join. This vortex reconnection results in a zig-zag lattice of flux lines in the plane of intersection. This configuration (Figure 8(b)) is energetically expensive and the energy is reduced by staightening out of the zigzags. Here the line tension or line energy or alternatively and equivalently the mutual repulsion between the adjacent curved segments, can be regarded as a driving mechanism. The sheet of flux lines that ensues from this process is densely packed in the plane of the paper (see Figure 8(c)). As a consequence, the mutual repulsion between the members of this "family" will lead to their separation into two adjacent parallel sheets, each having an equilibrium density as shown in Figure 8(d). We note that the distance between the flux lines in a sheet in (d) is greater than that initially existing in (a), although the number of flux lines has been conserved. Indeed

$$D_{final} = \frac{D_{initial}}{\cos(\Theta/2)},$$

hence the local magnetic flux density is reduced from B to $B\cos(\Theta/2)$. Clem refers to this latter process as flux consumption. It occurs because the transverse components of the magnetic flux density in the adjacent sheets vanish during the process of straightening of the flux lines. In effect the transverse components of one sheet can be regarded as annihilating with the oppositely directed transverse component of the neighbouring sheet.

Pursuing the proposed picture in the light of Maxwell's equation, $\nabla \times \vec{B} = \mu_0 \vec{j}$ we note that the sheet of longitudinal current $j_{||}$ between the two sheets of flux lines under scrutiny has vanished since these are now parallel. In a sense, the current

originally found in this space has been transfered to the adjacent volume since now the angle subtended by the two neighbouring flux line sheets with the two under consideration has increased from Θ to $\frac{3}{2}\Theta$, hence from critical or near critical to supercritical. Consequently, the entire process we have just described repeats and propagates inwards and outwards along the lattice of tilted flux line sheets. After application of a step function perturbation the process continues until the resulting configuration for $\Theta(x)$, hence $j_{\|}(x)$, has relaxed to subcritical. A continuous change of $\vec{H}_s$ may, of course, be regarded as a succesion of step function perturbations. In a dynamic steady state situation, such as encountered when a constant longitudinal flux flow voltage is measured along a current carrying ribbon, the sequence of events is periodic and continuous.

We now visualize that the flux cutting events just described occur at the surface of the sample. Let α denote the orientation of a flux line sheet just nucleated at the surface and $(\alpha - \Theta)$ the direction of the adjacent sheet before flux cutting. Consequently, the two sheet resulting from the flux cutting are directed along $\alpha - (\Theta/2)$. We focus on two extreme cases:

- all of the flux lines remain in the superconductor after the separation has taken place,
- the separation causes one of the flux line sheets to be expelled from the superconductor.

For a dynamic steady state to prevail, ejection of flux lines must take place, the loss to be replaced by the entry (creation) of a new flux line sheet directed along α. The flux line sheet that remains in the sample interacts with its neighbour

initially oriented along $\alpha - 2\Theta$ and the "information" is transmitted along the flux line lattice. For an infinite slab carrying a current $I > I_c$, the creation - expulsion sequence is taking place along both surfaces simultaneously. The lattice of flux lines can be regarded at any instant as comprising two sublattices, one moving along the positive, the other along the negative x axis, countermoving and continuously crossing each other. This is a convenient vantage point first proposed by Brandt [2,3]. Alternatively, one can view the events as a continuous shuttling back and forth between adjacent sheets of flux lines as first suggested by Clem [11].

In our experiment the configuration of flux lines is made to evolve continuously through these processes although we are not dealing with a dynamic steady state. The observations we present in the next chapter provide direct and unambiguous evidence that sheets of flux lines do indeed traverse each other.

Brandt [2,3] has shown, however, that the magnitude of the electric field which results from the picture just described is too small to account fo the measured longitudinal flux flow voltages. Clem [10] has proposed a double - cutting model which leads to better quantitative agreement with the data. We now sketch this model.

When the longitudinal current density $j_{||}$ is sufficiently large, the intermediate densely packed flux line sheet is unstable because of mutual repulsion of its members but also unstable towards the formation of left handed helices. We refer the reader to Figure 9 to follow the sequence of events now envisaged. The unstable left handed helices are driven to expand under the action of a Lorentz like force $\vec{j} \times \vec{B}$ and eventually come into contact with each other. Again, cutting and cross joining occurs at the points of intersection of the expanding helices. These events

lead to two "corrugated" sheets of flux lines which then reduce their energy content by straightening out. From inspection of the sequence of figures (a) - (f) we note that, in a sense, the series of processes has caused the original pair of flux lines to traverse each other and exchange places. By Maxwell's equation $\nabla \times \vec{B} = \mu_0 \vec{j}$, the longitudinal current density $j_{||}$ permeating the pair of flux line sheets has now reversed direction. The two sheets now consequently attract each other. The current density $j_{||}$ in the adjacent volume has however been increased, hence the attraction towards the neighbouring flux line sheets dominates and the perturbation propagates rapidly along the tilted flux line lattice. Focusing on the surface(s) we can again visualize a dynamic steady state of continuous periodic entry and exit of flux lines. The expelled flux lines now subtend an angle Θ with respect to $\vec{H}_s$, hence with respect to the flux lines entering the sample.

Two critical currents are now envisaged to play a role in type II superconductors:

- $j_{c\perp}$, flowing transverse to the flux lines is needed to overcome the opposition of pinning forces to the migration of the flux lines,
- $j_{c||}$, flowing along the flux lines is needed to drive non parallel flux lines to merge and intersect.

When $j_\perp > j_{c\perp}$, an electric field, denoted $E_\perp$, is generated by the transport of the flux lines. This feature was already envisaged in the classical critical state concept. When $j_{||} > j_{c||}$, and flux cutting occurs,an electric field, denoted $E_{||}$, is generated along the flux lines. This electric field arises from the displacement, straightening and other contorsions experienced by the flux lines as the sequence of events associated with the flux cutting process are unfolding. Here $E_{||}$ is regarded

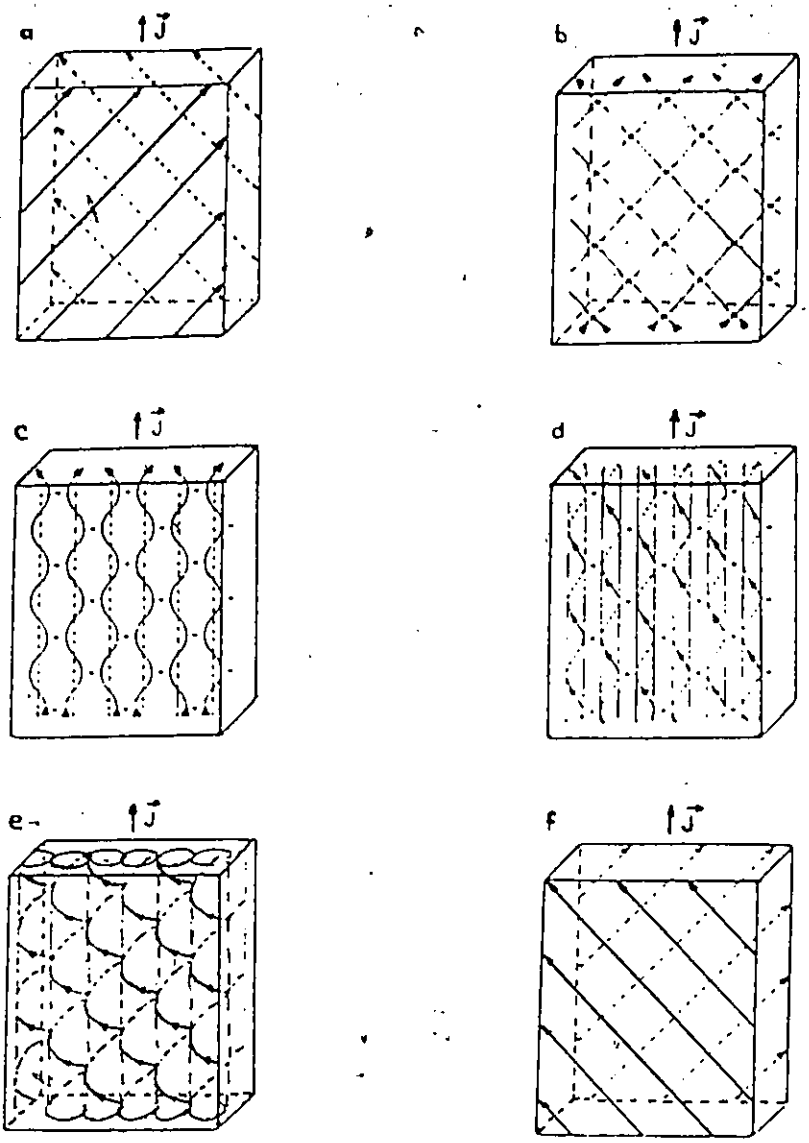

Figure 9: Two planes of vortices approaching each other (a), the first cutting (b), plane of zigzag vortices (c), their expansion into left-handed helical vortices (d), second cutting of helices (e) and the planes of parallel vortices moving apart from each other (f).

as a net electric field averaged over the duration of the flux cutting scenario and over the volume of the flux cutting event.

Introducing these ideas into Maxwell's equations, $\nabla \times \vec{B} = \mu_0 \vec{j}$ and $\nabla \times \vec{E} = -\partial \vec{B}/\partial t$, for infinite cylindrical geometry leads to :

$$\mu_0 J_\perp = -(\frac{\partial B}{\partial r} + B\frac{\sin^2 \alpha}{r}) \tag{17}$$

$$\mu_0 J_\parallel = B(\frac{\partial \alpha}{\partial r} + \frac{\sin \alpha \cos \alpha}{r}) \tag{18}$$

$$\frac{\partial B}{\partial t} = -\frac{\partial E_\perp}{\partial r} - E_\perp \frac{\cos^2 \alpha}{r} - E_\parallel(\frac{\partial \alpha}{\partial r} + \frac{\sin \alpha \cos \alpha}{r}) \tag{19}$$

$$\frac{\partial \alpha}{\partial t} = \frac{1}{B}(\frac{\partial E_\parallel}{\partial r} + E_\parallel \frac{\sin^2 \alpha}{r} - E_\perp(\frac{\partial \alpha}{\partial r} - \frac{\sin \alpha \cos \alpha}{r})) \tag{20}$$

where $\alpha(r)$ is the angle between flux density $\vec{B}(r)$ and the z axis. We stress that $E_\perp = 0$ when $0 \leq j_\perp \leq j_{c\perp}$ and $E_\parallel = 0$ when $0 \leq j_\parallel \leq j_{c\parallel}$.

In this scheme, energy dissipation is visualized to occur through flux migration, $E_\perp j_\perp$, and through flux cutting, $E_\parallel j_\parallel$. Regions where only the former is occurring are denoted T zones (flux transport zones), and where only the latter is occurring are denoted C zones (flux cutting zones). Regions where both processes are taking place simultaneously are denoted CT zones (flux cutting and flux transport zones). Regions where no energy dissipation occurs ($E_\perp = 0$ and $E_\parallel = 0$) are called O zones. We stress that in T zones, $j_\perp$ need not vanish and can vary with time. Here flux lines are migrating while retaining their orientation. This state of affairs has already been examined earlier. The important and novel features which now emerge are the following:

- the appearance of CT zones,
- the occurrence of pure flux cutting domains (C zones), and

- the possibility that in C zones $j_\perp$ does not have to vanish but can lie in the range $0 \leq j_\perp \leq j_{c\perp}$ and be allowed to vary with time.

Regions where $j_\perp$ was subcritical ($0 < j_\perp < j_{c\perp}$) were forbidden in the framework of the classical critical state.

In the next chapter we present some of our observations and examine these qualitatively in the framework of the models we have outlined above. We are developing a programme to compute the evolution of flux configurations in a hollow cylinder in accordance with the prescription presented above (Clem's formulation of Maxwell's equations) for the conditions prevailing in our experiments. This extremely difficult task is still in progress. Consequently, a quantitative analysis of our measurements must await a future date.

Chapter 4

4.1 Introduction

Much effort has been dedicated over the years to create experimental space where the magnetic field is negligible and indeed, in the limiting case, absolutely zero. The experiment we report here was motivated in part to explore a new scheme we concocted to achieve this objective. First, we describe the scheme.

We visualize that the ambient magnetic field (the Earth's field) has been screened out exploiting standard magnetic shielding techniques and cancelled out to a high degree of accuracy using Helmholtz coils. Now a hollow cylinder of a type II superconductor is cooled from T_c and becomes superconducting in this weak field environment. Clem et al. have shown [13] that the transverse component of the magnetic flux threading the wall of a thin walled type II superconducting tube can be reduced by sending a current along the wall. The Lorentz force, $j_z B_\perp$, drives the flux lines to one edge of the tube where they can be regarded as mutually annihilating or being expelled. The impressed current, having accomplished the purpose, is then "removed". The axial component of the ambient magnetic field still remains

however. We focus on ways to reduce or eventually remove this component of the magnetic flux inside the cavity of the hollow cylinder.

Our approach is conceptually straightforward. We cause the magnetic flux density along the inner wall of the hollow cylinder to increase by superimposing an azimuthal component $H_\phi(R_i)$ on the existing $H_z(R_i)$. Presumably, $H_z(r)$ is uniform in the hollow, but this is not pertinent. The important feature is that the increase in

$$\vec{H}(R_i) = \hat{z}H_z(R_i) + \hat{\phi}H_\phi(R_i)$$

causes flux lines to nucleate along the inner surface of the wall and penetrate into it. Now each of these flux lines removes a quantum of axial flux from the hole and transfers it to the wall. As a result the axial flux density in the hole is made to diminish as helical flux lines are being "pumped" from the cavity into the wall. At this stage, we have reduced B_z in the hole at the price of increasing $B_\phi(r)$, and $B(r) = (B_z^2 + B_\phi^2)^{\frac{1}{2}}$. We now reduce $H_\phi(R_i)$ to zero. Our hope is that a large fraction of the flux lines "pushed" from the cavity into the wall will remain trapped (pinned) there when $H_\phi(R_i)$ is made to vanish. Thus at the end of the cycle of $H_\phi(R_i)$ we expect to have depleted the cavity of a substantial fraction of its axial flux. We first report on our exploration of the "merits" of this scheme. The verdict on the "effectiveness" of this novel approach is not encouraging. In the course of these measurements however we encountered fascinating and novel behaviour which shed light on the flux cutting process. We also present and discuss these new and interesting aspects.

4.2 Evolution of Axial Magnetic Flux in the Hole

Our "ultimate" objective is to reduce the axial flux density initially threading the cavity of a hollow cylinder starting with a value previously rendered negligible by standard screening and cancellation techniques. For experimental expediency and convenience we chose to test our proposed technique in the regime of appreciable ambient magnetic fields $H \geq H_{c1}$. Consequently, we examine the behaviour arising when our sample became superconducting by cooling from T_c to 4.2 K in various applied magnetic inductions $\mu_0 H_{||}$ ranging from a few milliteslas to $\approx$ 250 milliteslas.

The thick curve in Figure 10 displays the evolution of the axial flux density in the hole, B_{zh}, as the total magnetic field intensity $\vec{H}_s = \hat{z}H_z + \hat{\phi}H_\phi$ is made to increase by superimposing on the existing H_z an azimuthal component H_ϕ generated by the toroidal magnet coil. For convenience we present $\Delta B_{zh} = B_{zh} - \mu_0 H_{||}$ versus $\langle B_\phi \rangle_{appl}$, the applied azimuthal magnetic induction averaged over the appropriate cross section of the wall. We note that, as anticipated, the axial flux density in the hole is initially reduced by this procedure. This result is in harmony with the accepted picture that the rise in $\mid \vec{H}_s(R_i) \mid$ causes flux lines to nucleate along the surface(s) of the wall and to penetrate into the material. Each of the flux lines created along the inner radius R_i however removes a quantum of axial flux from the hole. Thus the axial flux in the hole, $\Phi_{zh} = B_{zh}\pi R_i^2$, is being depleted as the transfer of flux lines to the wall progreses.

With this simple picture in mind, it is then surprising to observe that eventually, when H_ϕ attains large values, the process of migration of axial flux from the hole into the wall not only ceases but reverses. This behaviour emerges from inspection

$$\mu_0 H_{\|} = 70\ mT$$

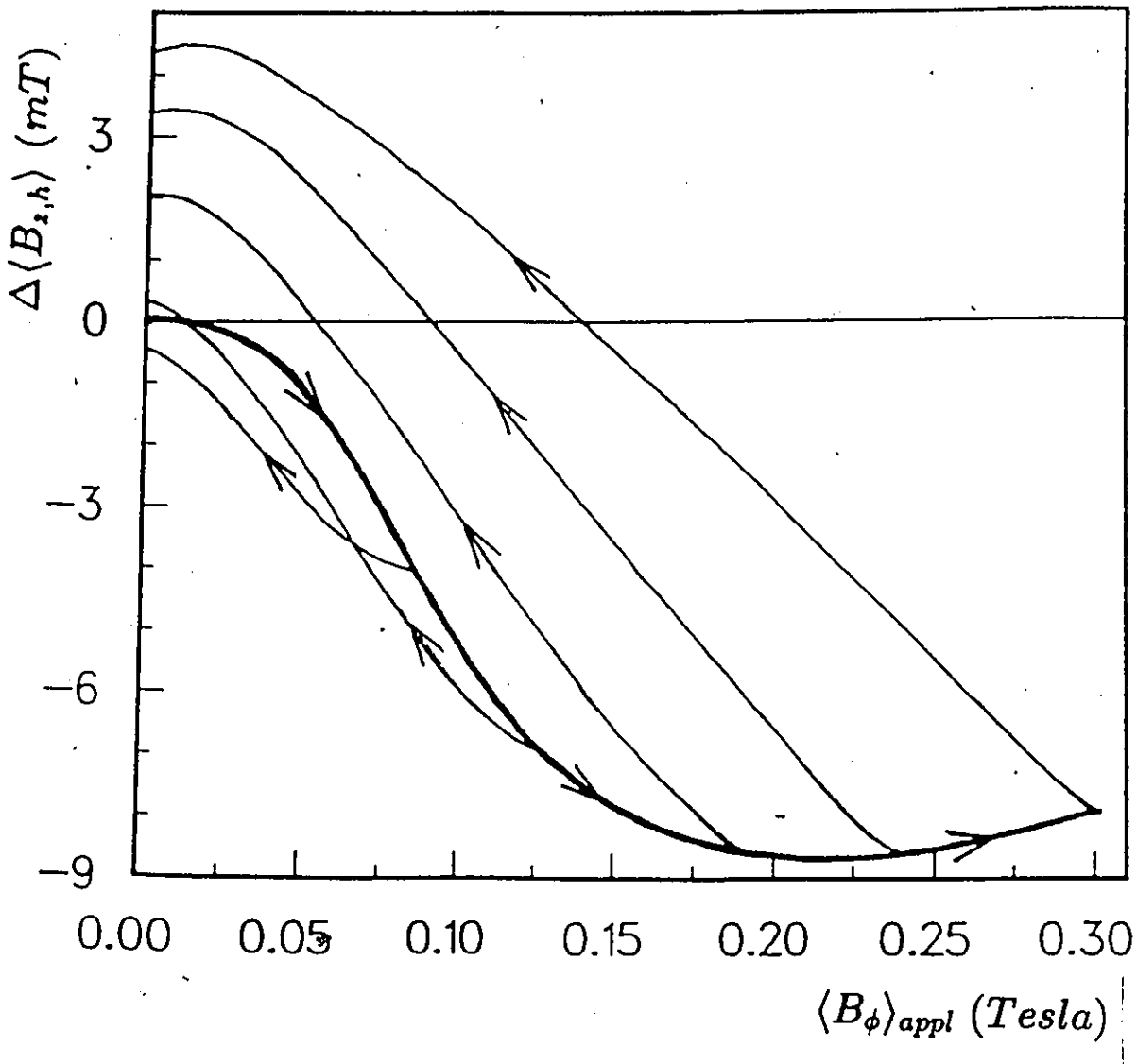

Figure 10: Evolution of the axial flux density in the hole, B_{zh}, versus the azimuthal applied field $\langle B_\phi\rangle_{appl}$

of the thick curve (see Figure 10) whose slope is seen to change from negative to positive. In the positive region axial flux is leaving the wall and entering the hole although flux lines are being "pumped" from the hole into the wall by the increase in H_ϕ. We will return to this fascinating behaviour later in this chapter.

At various points along the thick curve in Figure 10 the sweep of H_ϕ is interrupted and reversed. As H_ϕ is removed, flux lines are released from the wall into the cavity, hence, as expected, B_{zh} rises. One might say that some of the flux lines pushed out of the hole into the wall during the rise in H_ϕ (hence the rise in $\mid \vec{H}_s \mid$) are now sliding back into the hole. The process should not be reversible since some of the flux lines that have migrated into the wall are expected to be held captive by the pinning sites there and not permitted to return during the downswing.

A careful inspection of the family of loops displayed in Figure 10 confronts us with several unexpected (although interrelated) results. We examine these, one by one, starting with the behaviour for swings of H_ϕ of small amplitude. It may be useful to indicate that in the framework where flux lines experience pinning but undergo no cutting (the classical critical state) we can predict that between 1/2 (Bean limit) and 2/3 (Kim - Anderson limit) of the flux lines transferred from the hole to the wall would remain there after a swing of $H_\phi < H_\phi^*$ where H_ϕ^* is the field for full penetration of the flux disturbance. We note that for swings of small amplitude (the smallest loop in Figure 10 is typical) only a small fraction ($\leq 1/4$) of the axial flux deported from the hole into the wall during the upswing remains in the wall after the cycle has been completed. This result is most disappointing as regards our scheme of substantially reducing the axial flux in hollow cylinders by the application and removal of an azimuthal field. It seems that flux cutting comes

into play and instead of providing assistance, this mechanism conspires to defeat our goal.

Even more surprising in our view, are the characteristics of the curves traced for swings of $\langle B_\phi \rangle_{appl} > \mu_0 H_\phi^* \approx 0.1$ Tesla. We note that the locus of B_{zh} versus H_ϕ has switched from clockwise for small excursions of H_ϕ to counterclockwise for excursions of larger amplitudes. This reversal is associated with the startling observation that more axial flux is made to enter the hole during the downswing than was removed from the hole during the upswing. Clearly, here the wall acts as an unusual philantropist, donating more axial flux than it has received. Some process is taking place in the wall which enables it to be such a benefactor and act as a source of axial flux.

Finally we note that this generous behaviour appears to be exhaustible and indeed to suffer transformation. From inspection of the return portion of the family of curves of large amplitude displayed in Figure 10 we notice that the curves flatten out and appear to turn around as H_ϕ approaches zero. Thus the sliding of axial flux from the high flux density wall into the hole ceases and indeed reverses direction.

We now focus on the net change in the axial flux in the hole, $\Delta\langle B_{zh} \rangle_{net}$, and its dependence on the magnitude of the excursion of $\langle B_\phi \rangle_{appl}$. The data obtained for one chosen static axial field $\mu_0 H_\parallel = 70$ mT are displayed in Figure 11 and is representative of the behaviour encountered at all the axial fields over the range we have explored (up to 0.25 Tesla). Small excursions of $\langle B_\phi \rangle_{appl}$ effect no significant change in $\Delta\langle B_{zh} \rangle_{net}$ since only a small amount of flux is made to enter or leave the wall during these weak swings. It is of interest that the magnitude of $\Delta\langle B_{zh} \rangle_{net}$ grows essentially linearly over the intermediate range $0.04 \leq \langle B_\phi \rangle_{appl} \leq 0.1$ Tesla.

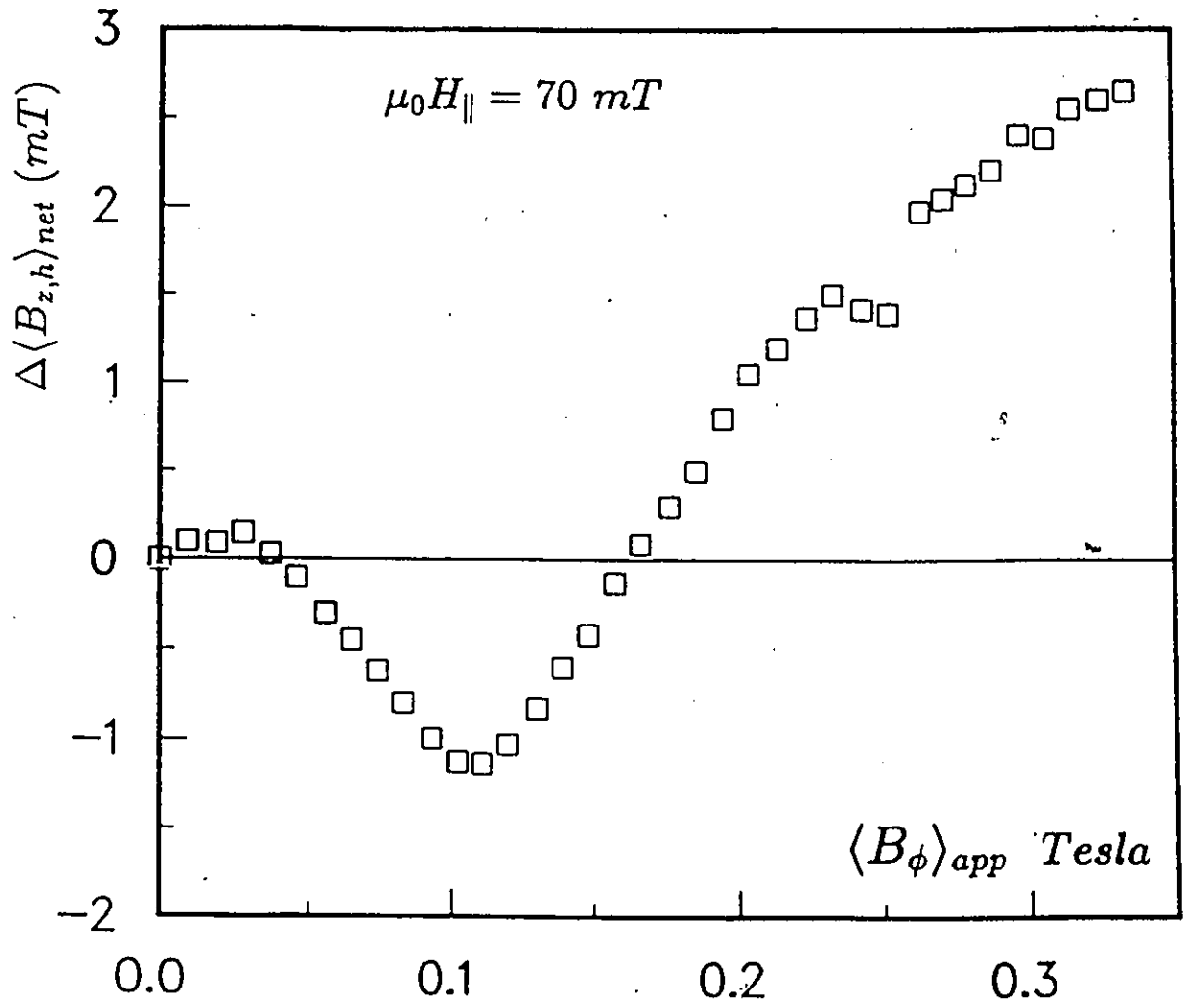

Figure 11: Net change of the axial flux density in the hole $\Delta\langle B_{zh}\rangle$ versus azimuthal applied field $\mu_0\langle H_\phi\rangle$

This rise terminates abruptly when the swing of H_ϕ attains the value of the full penetration field H_ϕ^*. We estimate $B_\phi^* = \mu_0 H_\phi^* \approx 0.1$ Tesla from magnetization data to be presented later in this chapter. The classical critical state model (no flux cutting) would predict a plateau at the maximum (saturation) value attained for $\langle B_{zh} \rangle_{net}$ versus H_ϕ beyond H_ϕ^*. We witness instead a monotonic evolution of $\langle B_{zh} \rangle_{net}$ from a net deficit to a net surplus situation for swings of H_ϕ of increasing magnitude. The data suggest that a leveling off is on the horizon, but our present setup is inadequate to explore these regions of phenomena.

4.3 Evolution of the Axial Magnetic Flux in the Wall

In the preceding section we have examined the evolution of axial flux contained in the hole during excursions of various amplitudes of an azimuthal magnetic field H_ϕ (generated by the toroidal magnet coil) while the external magnetic field $H_\parallel$ was maintained constant. We now look at the behaviour of the axial flux permeating the wall which accompanies the changes taking place in the cavity.

The thick curve displayed in Figure 12, traced at the same time as the thick curve of Figure 10, shows the evolution of the axial flux density in the wall, denoted $\langle B_{zwall} \rangle$, during the application of H_ϕ, hence during the rise in $\mid \vec{H}_s \mid$. Each of the five open loops in Figure 12 was observed simultaneously with the open loop of Figure 10 of corresponding horizontal amplitude.

These data present the change of axial flux detected by the balanced pickup coil which embraces the "waist" of the hollow cylinder, hence surrounds both the

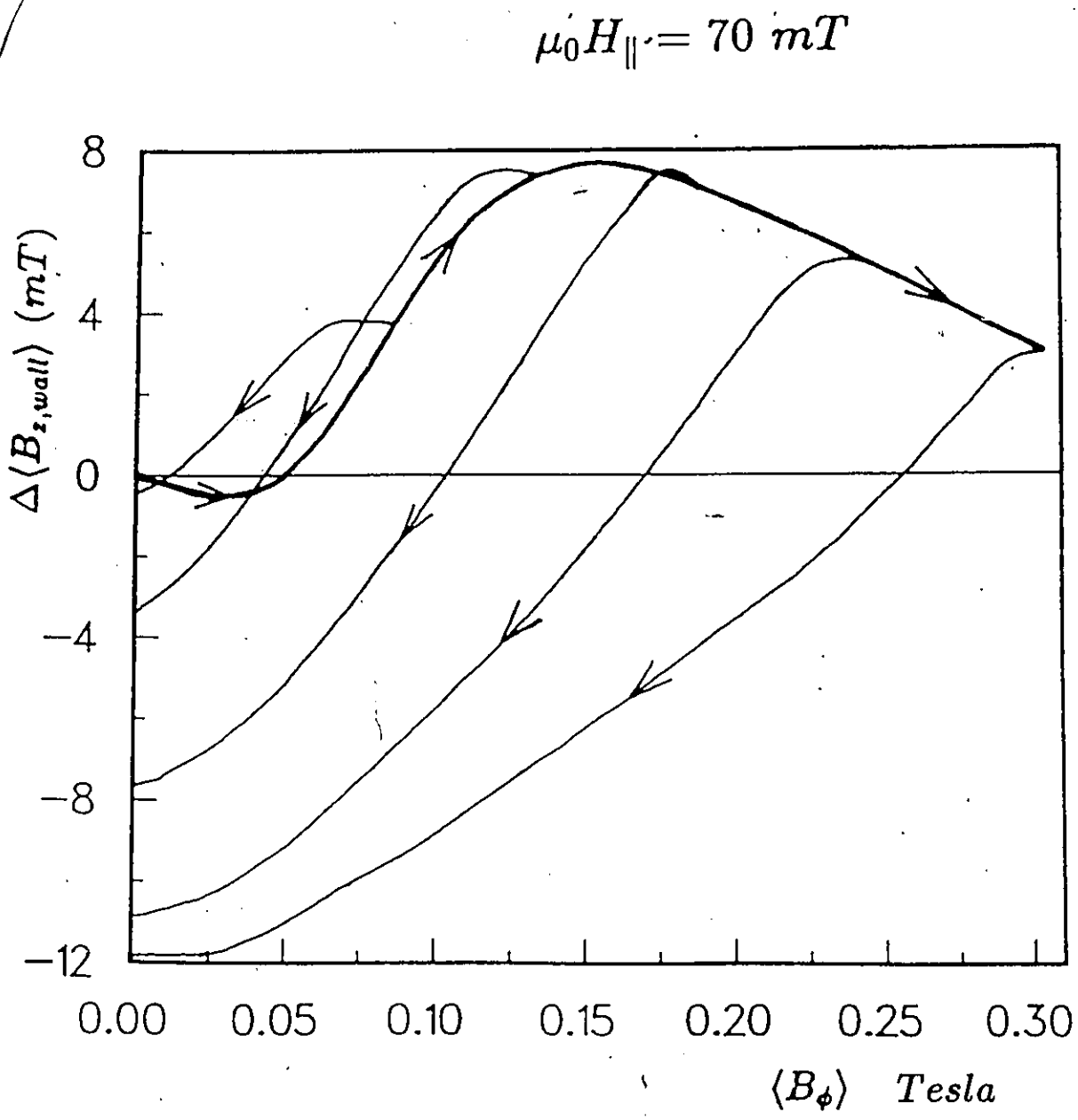

Figure 12: Evolution of the axial flux density in the wall $\langle B_{z,wall}\rangle$ versus the azimuthal applied field $\langle B_\phi\rangle_{appl}$

wall and the hole of the sample. The vertical axis has been scaled by a factor $R_o^2/(R_o^2 - R_i^2)$ in order to assign the entire calibrated measured signal to the wall. Our viewpoint here is that any axial flux removed from the hole and transferred to the wall and vice versa generates no signal in this pickup coil. The "raw" data displayed here as $\Delta\langle B_{z,wall}\rangle$ is regarded as representing the resultant of the following:

- the entry or exit of axial flux through the outer surface, and
- the consumption and rotation of axial flux by flux cutting processes.

Inspection of the thick curve in Figure 12 reveals two salient features:

- the curve first traces a valley,
- the curve after traversing a summit shows an unmistable, continuous descent.

We stress that, all along, axial flux is being made to enter the wall through the outer surface (here we ignore events occurring along the inner surface since these do not contribute to the signal we are examining). Consequently, in the absence of other processes, we expect a continuous, monotonic rise, albeit with diminishing slope, of $\langle B_{z,wall}\rangle$ versus H_ϕ. The appearance of two regions with negative slopes then carries the clear signature that flux cutting is taking place in a rather dramatic way.

The return portions of the five half cycles displayed in Figure 12 (thin lines) confirm the phenomenon encountered when we focused on the behaviour in the hole.

(a) Axial flux "pumped" into the wall through the outer surface during the rise in H_ϕ, which has survived the flux cutting process, is now being released to the outside

world.

(b) Also after large excursion of H_ϕ, some of the axial flux originally permeating the wall is now being carried out by the emerging flux lines.

As a consequence of the large excursions of H_ϕ, a deep valley has been gouged out of the initially uniform $B_z(r)$ profile in the wall. This valley together with any azimuthal flux made to "rotate" along the z axis by the flux cutting processes are the sources of the rise of axial flux in the cavity noted in the previous section.

The net change of axial flux in the wall, $\Delta\langle B_{z,wall}\rangle_{net}$, ensuing from half cycles of H_ϕ (such as displayed in Figure 12) is presented in Figure 13. The initial flat region indicates that swings of H_ϕ of small amplitude leave the $B_z(r)$ profile essentially intact (no valleys or peaks are left behind). Our observations in the hole over the corresponding range of cycles showed however, that not all of the axial flux removed from the hole during the upswing was returned during the downswing. These two sets of observations lead us to the following conclusions. The net reduction of flux in the hole generated by the cycles of small amplitude arises not because pinning retains this flux in the wall but rather because this flux was consumed in the wall by flux cutting.

We note from Figures 12 and 13 that excursions of amplitudes $H_\phi > H_\phi^*$, the full penetration field, leave the wall with a deficit in axial flux. This deficit is seen to increase with the amplitude of the swing. We have seen earlier that excursions of large amplitude left the hole richer in axial flux (see Figures 10 and 11). These observations then confirm and complement each other and lead to a picture of a deep valley in the $B_z(r)$ profile in the wall, some of the flux originally permeating this valley, now threading the hollow of the cylinder. Simple estimates of the depth

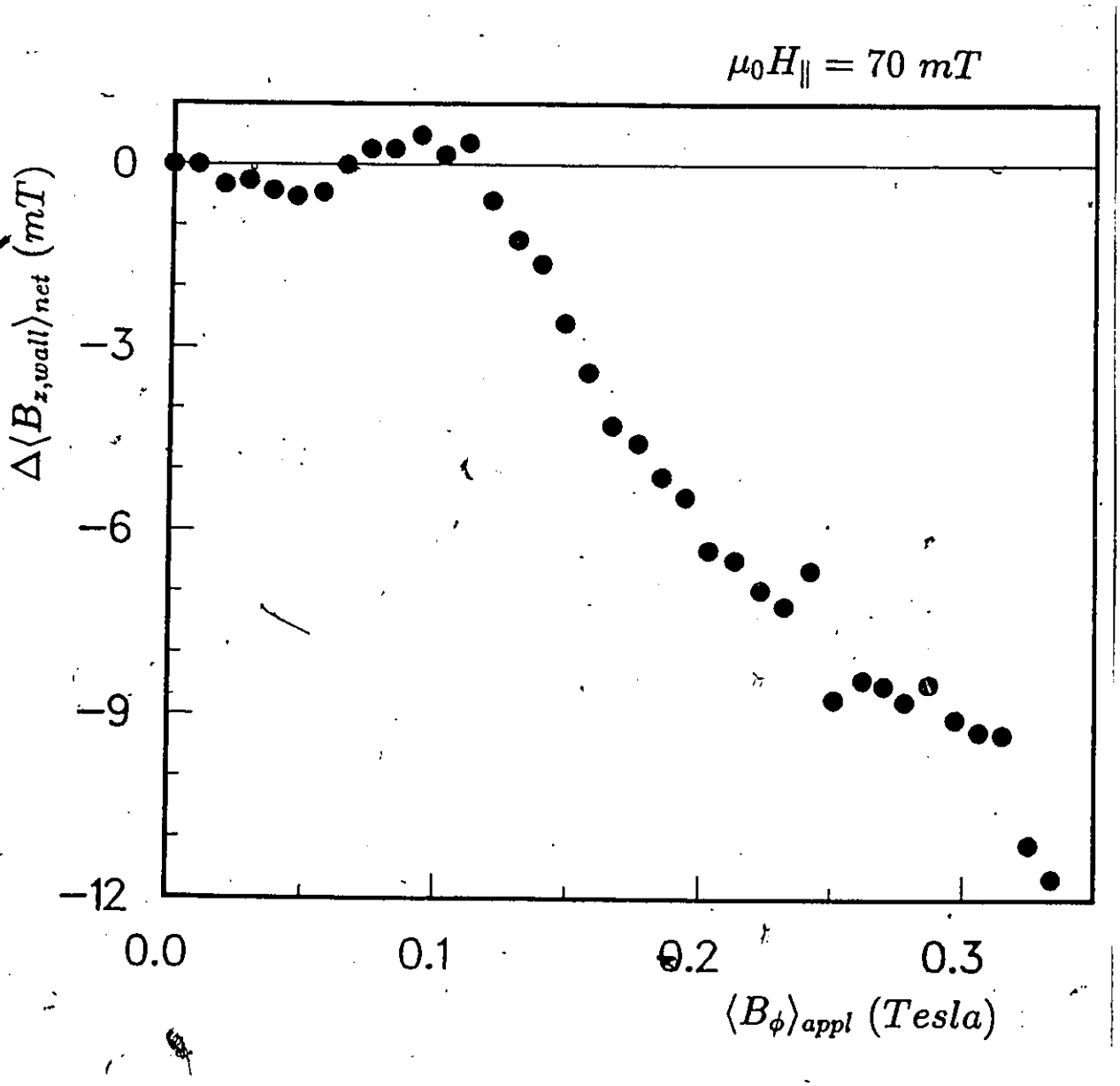

Figure 13: Net change of the axial flux density in the wall $\Delta\langle B_{z,wall}\rangle_{net}$ versus azimuthal applied field $\langle B_\phi\rangle_{appl}$

of this valley indicate that, at low axial fields such as $H_{||} \leq 70$ mT, the bottom of the valley may be free of axial flux. This is indeed an amazing result. Further we note that the data curves show no strong indication that this trend is leveling off.

4.4 Effect of Flux Density on the Flux Cutting Phenomena

It is of interest to explore the influence of flux line density on the evolution of the flux configuration in the hole and the wall of the hollow cylinder in the flux cutting regime. Consequently, we have examined this behaviour when the sample is subjected to half cycles of azimuthal field in several static axial fields $H_{||}$ over a broad range extending from zero to 350 mT. Observations in a "low" field, $\mu_0 H_{||} = 70$ mT, have already been presented. We now display measurements made at a slightly lower field, $\mu_0 H_{||} = 50$ mT and at an appreciably larger field, $\mu_0 H_{||} = 250$ mT, for comparison in Figures 14 and 15. To avoid clutter, we have shown the locus of the measured quantities during the upswing of H_ϕ only.

For completeness we have also displayed the evolution of the azimuthal magnetization, $\mu_0 \langle M_\phi \rangle = \langle B_\phi \rangle - \langle B_\phi \rangle_{appl}$, where $\langle B_\phi \rangle$ is the spatial average of azimuthal flux density $B_\phi(r)$. First, we note that the presence of a strong axial flux causes a significant reduction in the magnitude of $\langle M_\phi \rangle$ when $H_\phi > H_\phi^*$. This behaviour has been reported previously in other situations by our group. It is of interest because it means that, at large magnetic fields, the longitudinal critical current density, j_{cz}, is increased when B_z is made larger. This behaviour has been intimately linked by

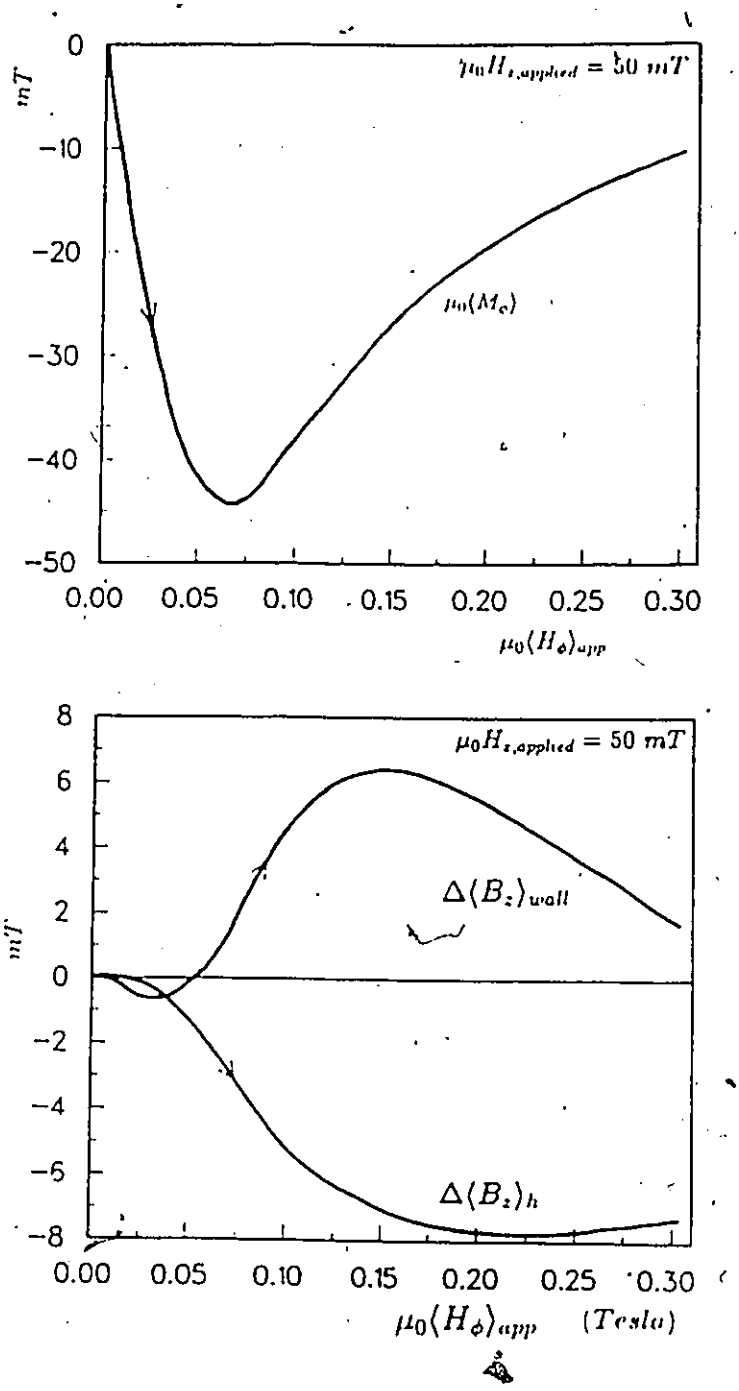

Figure 14: Magnetization curves $\mu_0 M_\phi$ and $\Delta\langle B_{z,hole}\rangle$, $\Delta\langle B_{z,wall}\rangle$ in increasing azimuthal field $\langle B_\phi\rangle$ for applied static field $\mu_0 H_\parallel = 50$ mT.

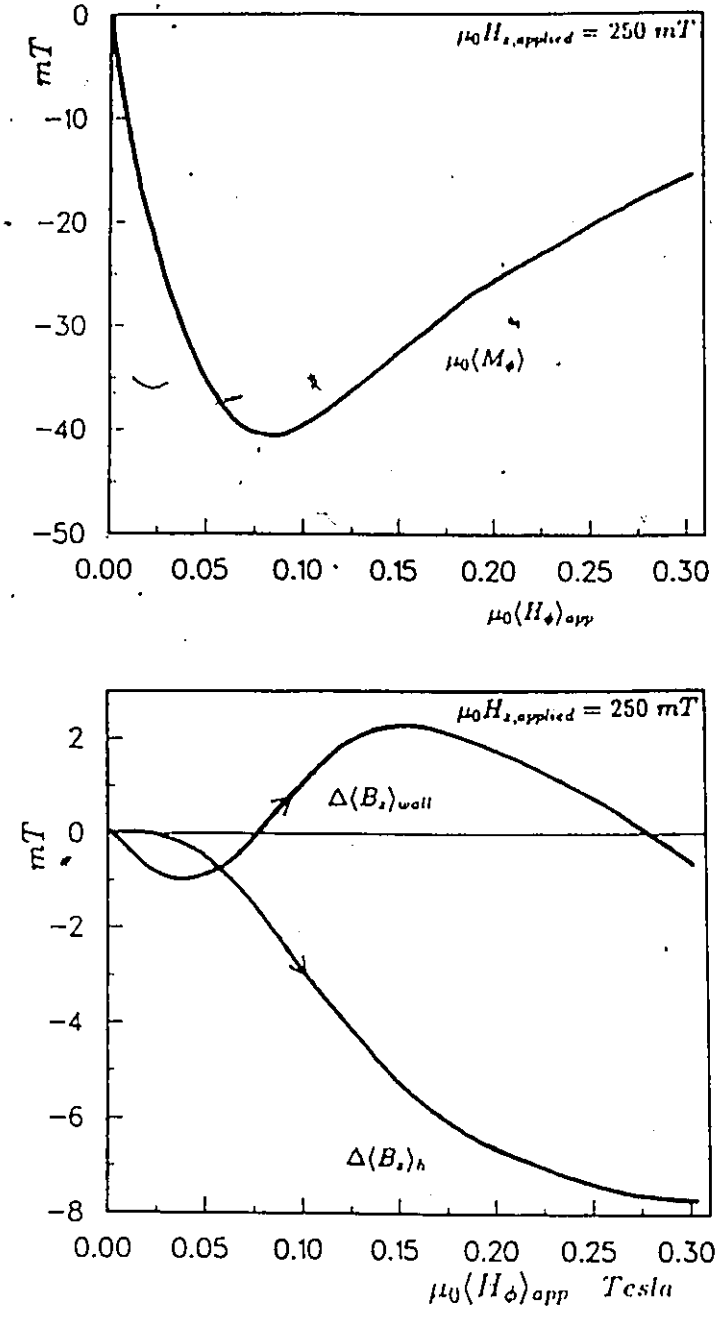

Figure 15: Magnetization curves $\mu_0 M_\phi$ and $\Delta\langle B_{z,hole}\rangle$, $\Delta\langle B_{z,wall}\rangle$ in increasing azimuthal field $\langle B_\phi \rangle$ for applied static field $\mu_0 H_\parallel = 250$ mT.

Clem to the flux cutting critical current density, $j_{c\|}$.

Figures 14 and 15 confirm the phenomena reported above. The two features which carry the clear signature of flux cutting, namely the regions of negative slope in the locus of $\langle B_{z,wall} \rangle$ versus $\langle B_\phi \rangle_{appl}$, are even more dramatic in the stronger $H_\|$. In particular, the valley is evidently more pronounced on a relative and also on an absolute scale in the stronger $H_\|$.

We note that $\langle B_z \rangle_{hole}$ seems to have attained a plateau at the end of the upswing in the stronger $H_\|$. It is tantalizing to speculate, that if yet larger H_ϕ were available, an upward movement would be detected.

4.5 Effect of Helical Flux Configuration

The configuration of the magnetic flux in the wall of the cylinder becomes increasingly complicated as the upsweep in H_ϕ progresses. As a consequence, the "initial" configuration when the sweep of H_ϕ is interrupted and reversed is extremely convoluted. As a result, it is a formidable challenge to unravel the sequence of events encountered during the downsweep. It is certainly desirable to start a measurement with the simplest configuration possible. For the upsweep, this is achieved by letting the sample become superconducting in a uniform, static longitudinal magnetic field. The hole and the wall of the cylinder is then threaded by a uniform density of axial flux. We can establish a relatively simple initial configuration of helical flux lines by letting the sample become superconducting through cooling from T_c to 4.2 K in a stationary helical magnetic field generated by the superposition of $H_\|$ and H_ϕ. We can then examine the evolution of this configuration of cylindrical sheets

of helical flux lines when H_ϕ is removed.

In Figures 16 and 17 we display the evolution of $\langle M_\phi \rangle$, $\langle B_{z,hole} \rangle$ and $\langle B_{z,wall} \rangle$ as H_ϕ is removed starting from 300 mT in the presence of $\mu_0 H_\parallel = 50$ and 250 mT. These data should be compared with each other and with the corresponding curves of Figures 14 and 15 since in a sense they show the reverse "side" of the behaviour under scrutiny.

Although now the entire flux line lattice consists of helical flux lines, the axial component of the magnetic flux density $B_z(r)$ is initially uniform. As the ambient azimuthal field H_ϕ is removed, flux lines are released through the inner and outer surfaces of the wall. Each of the flux lines "sliding" into the hole adds a quantum of axial flux to that already present in that finite reservoir. It is then not surprising that, initially:

- $\langle B_{z,hole} \rangle$ is seen to rise,
- $\langle B_{z,wall} \rangle$ is seen to diminish

as H_ϕ is reduced. The behaviour here, at first glance is simply the reverse of that witnessed in Figures 14 and 15 where flux lines were made to enter the wall.

A novel and startling feature dramatically evident at large $H_\parallel$ (see Figure 17) is that the locus of $\langle B_{z,hole} \rangle$ and $\langle B_{z,wall} \rangle$ both turn around as H_ϕ approaches zero. We are now confronted with an interesting paradox.

On one hand, helical flux lines are continuously being released from the wall into the hole since $H_s(R_i)$ is made to decrease. Experimentally, this exodus is confirmed by the evolution of the azimuthal flux $\langle B_\phi \rangle$, hence the azimuthal magnetization $\langle M_\phi \rangle$, versus H_ϕ, which is displayed at the top of the figures. Indeed, from these

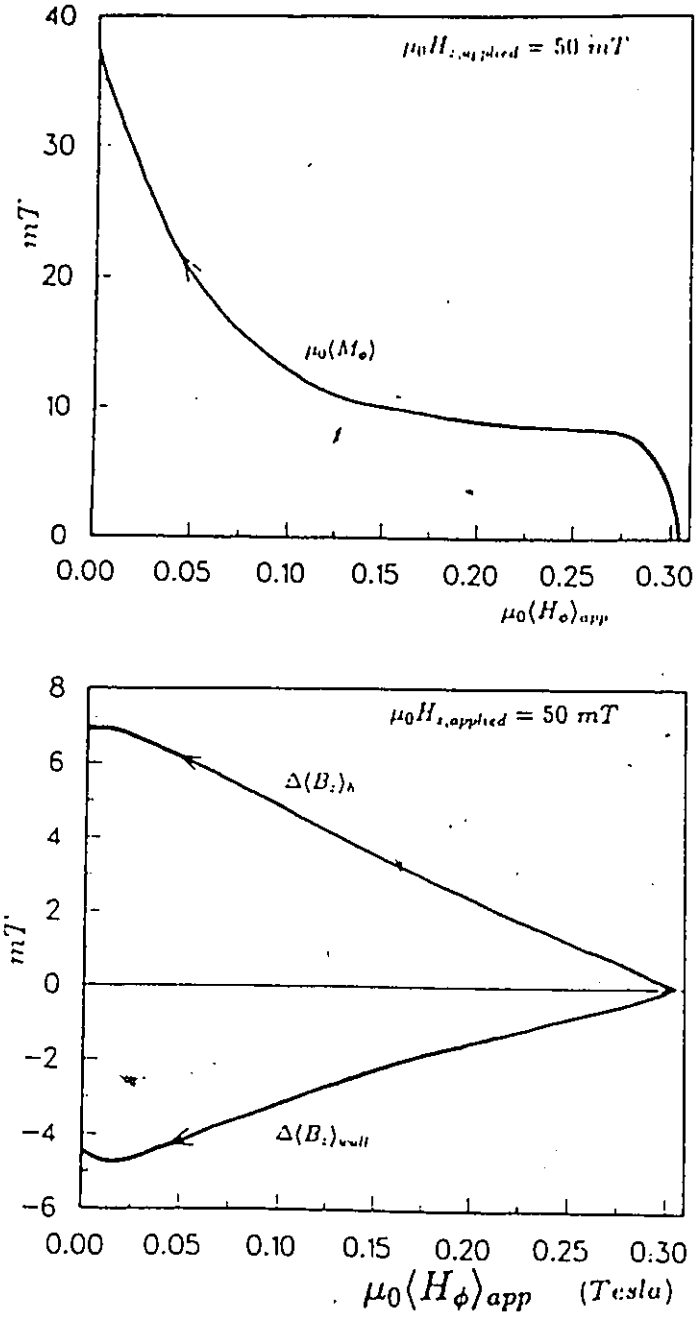

Figure 16: Magnetization curves $\mu_0 M_\phi$ and $\Delta\langle B_{z,hole}\rangle$, $\Delta\langle B_{z,wall}\rangle$ in decreasing azimuthal field $\langle B_\phi\rangle$ for applied static field $\mu_0 H_{||} = 50$ mT.

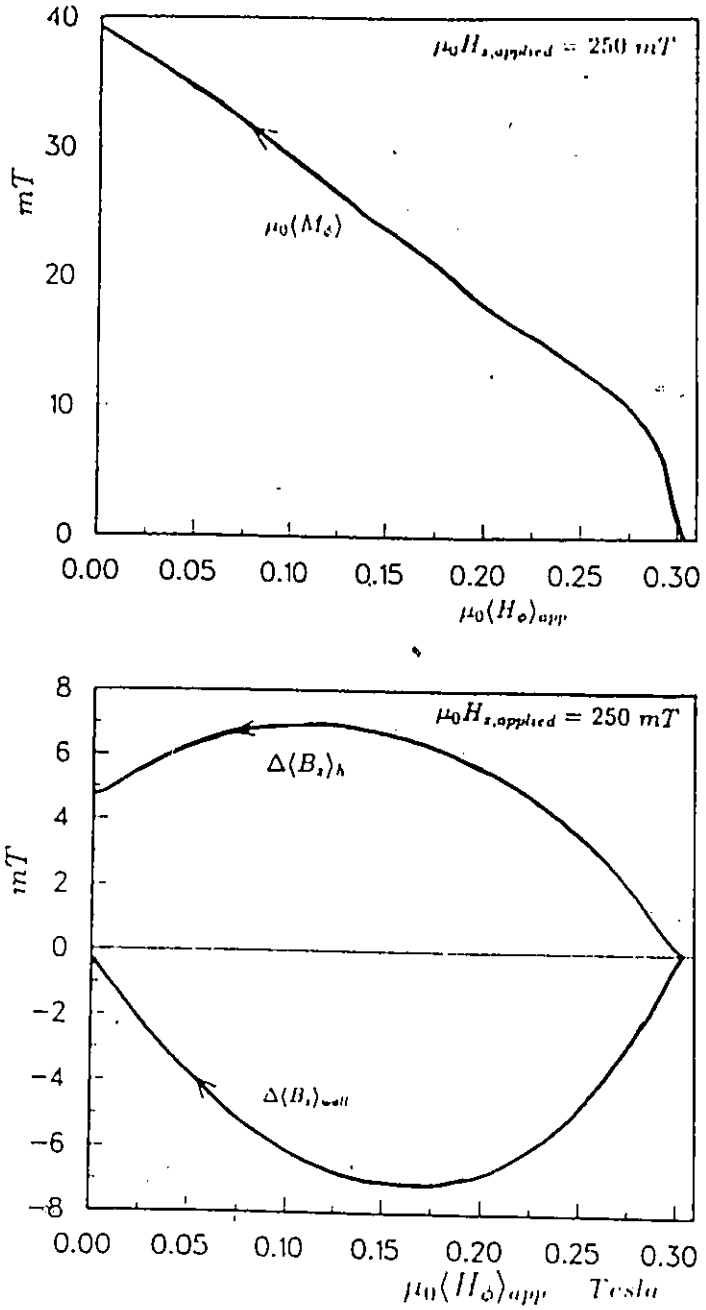

Figure 17: Magnetization curves $\mu_0 M_\phi$ and $\Delta\langle B_{z,hole}\rangle$, $\Delta\langle B_{z,wall}\rangle$ in decreasing azimuthal field $\langle B_\phi\rangle$ for applied static field $\mu_0 H_\parallel = 250$ mT.

data the rate of release of flux from the wall is seen to be the greater for the stronger $H_{\|}$. The flux lines released into the hole must be helical since, (i) $\vec{H}_s(R_i)$ is helical, and (ii) the configuration of the flux line lattice in the wall is helical. Again, we stress that each of the flux lines released into the hole carries a unit of axial flux into that enclosure.

On the other hand we witness that:

(a) the axial flux in the hole is now decreasing, and

(b) the axial flux in the wall is now correspondingly increasing.

We must infer from these facts that flux lines are leaving the hole and entering the wall. The flux lines moving out of the hole must be helical since the magnetic field inside the hole along the inner surface of the wall is helical.

We are then inexorably led by our observations, in the framework of accepted ideas, to a picture of countermoving cylindrical sheets of helical flux lines traversing each other along the inner surface of the wall. The net transfer of axial flux resulting from this counterflow is outwards at R_i when H_ϕ is entering the range of low values during its decrease.

Presumably, the behaviour along the outer surface of the wall is the mirror image of the phenomena taking place along its inner surface. Thus, along the outer surface, the net flow of axial flux must be inwards since we observe an increase in $\langle B_{z,wall} \rangle$ with the external pickup coil. (We remind the reader that transfer of flux between the hole and the wall will yield no signal in this detector. The inner axial pickup coil in the closed space of the cavity directly monitors transfers of axial flux between the wall and the hole.) We are thus compelled to visualize a counterflow of cylindrical sheets of helical flux lines at the outer surface of the hollow cylinder

also. The counterflow at R_i and R_o leads to a net increase in the axial flux in the wall although the total flux density in the material is made to decrease.

At first glance, the two-way flow picture we have developed to account for the observations appears to contain a contradiction. Since each flux line carries a unit of flux ϕ_0, the decrease of axial flux in the hole indicates that $\Delta n''$, the number of flux lines entering the wall is greater than $\Delta n'$, the number of flux lines leaving the wall. The total magnetic flux in the wall however is diminishing since

$$\mid \Delta\Phi_\phi \mid = \Delta\langle B_\phi \rangle Z(R_o - R_i)$$

the magnitude of the decrease in the amount of azimuthal flux is greater than

$$\Delta\Phi_z = \Delta\langle B_{z,wall} \rangle \pi(R_o^2 - R_i^2)$$

the increase in the amount of axial flux.

The solution to this "quandary" is found in the helical character of the flux lines. At all times, the helicity of the flux lines leaving the wall is greater than the helicity of the flux lines entering the wall. Consequently, N_c', the number of circumferential circuits traced by the former is greater than N_c'', the number of circuits covered by the latter. Thus the total azimuthal flux $\Phi_\phi' = N_c'\phi_0$ contained by a departing flux line is greater than $\Phi_\phi'' = N_c''\phi_0$ for a flux line entering the wall. For the remarkable situation under scrutiny we find that:

$$\Delta n' N_c' > \Delta n'' N_c'' \tag{21}$$

although $\Delta n' < \Delta n''$.

In our experiment,

$N_c' > N_c''$ for H_ϕ decreasing and

$N_c' < N_c''$ for H_ϕ increasing.

Our interpretation of the startling behaviour we have encountered is in harmony with the detailed pictures of flux cutting described in the preceding chapter. Indeed our observations provide the first direct support for these descriptions of flux cutting events. Our explanation is evidently incomplete since it provides no reason why in some circumstances the number of flux lines entering the wall during the counterflow exceeds the number of those leaving it while under other conditions this is not the case.

Finally, we note that a reversal in the evolution of the axial flux in the hole and in the wall can also be discerned during the increase of H_ϕ in low $H_\parallel$ (see Figures 10 and 14) although there the changes of slope are less prominent. The picture of countermoving cylindrical sheets of flux lines therefore applies to these observations as well, although now

$$\Delta n' N_c' < \Delta n'' N_c''$$

and

$$\Delta n' > \Delta n''.$$

We may speculate that counterflow of flux lines is taking place whenever flux cutting is occurring, hence wherever $j_\parallel > j_{c\parallel}$ regardless of the values of H_ϕ and $H_\parallel$ that may come into play. Various circumstances however will determine whether $\Delta n'$ is greater or less tahn $\Delta n''$ in a way which needs to be elucidated.

4.6 Conclusions and Summary

We set out to reduce the axial flux threading the cavity of a hollow cylinder of a type II superconductor in a static axial field $H_\parallel$ by subjecting the sample to a half

cycle of azimuthal field H_ϕ. We expected that a sizeable fraction of the axial flux transferred to the wall by vortex nucleation and migration during the upsweep of H_ϕ would (i) remain imprisoned there by flux pinning after the downsweep of H_ϕ, and (ii) be "consumed" by flux cutting in the wall during the swing of H_ϕ. To our consternation, we found that most of the axial flux removed from the hole during the application of H_ϕ returned there when H_ϕ was brought back to zero. Indeed, to our surprise, we discovered that large swings of H_ϕ would cause a net increase in the axial flux in the hole.

We had designed an arrangement where all of the pertinent magnetic quantities are measured simultaneously. These are the axial flux density in the hole, $\langle B_{z,hole} \rangle$, the axial flux density in the wall, $\langle B_{z,wall} \rangle$, and the azimuthal flux density in the wall, $\langle B_\phi \rangle$. From our observations of the evolution of these quantities we identified features which bear the "clear" imprint of flux cutting. We examined the behaviour starting with the simplest helical configuration of magnetic flux we could devise and establish. We also investigated the effect of flux density on the flux cutting processes. These studies led us to a most remarkable occurrence, namely that flux lines are entering the wall of the sample when flux is leaving it (and vice versa). We have shown that these observations provide evidence and support for detailed models developed by other workers of the flux cutting sequence of events between adjacent sheets of flux lines. In these models, the sheets of flux lines or sublattices can be seen as traversing each other. In our work, however, we have encountered a counterflow of flux lines of a most unusual character. We are then left with a new question. What factors give rise to the special regime of counterflow we have discovered?

Bibliography

[1] E.H. Brandt. Continuous vortex cutting in type ii superconductors with longitudinal current. *Journal of Low Temperature Physics*, 39:41–61, 1980.

[2] E.H. Brandt. Longitudinal critical current in type ii superconductors. 1. helical vortex instability near the surface. *Journal of Low Temperature Physics*, 44:59–72, 1981.

[3] E.H. Brandt. Longitudinal critical current in type ii superconductors. 2. helical vortex instability near the surface. *Journal of Low Temperature Physics*, 44:33–57, 1981.

[4] E.H. Brandt, J.R. Clem, and D.J. Walmsley. Flux-line cutting in type ii superconductors. *Journal of Low Temperature Physics*, 37:43–55, 1979.

[5] J.R. Cave and J.E.Evetts. Static electric potential structures on the surface of a type ii superconductor in the flux flow state. *Phylosophical Magazine B*, 37(1):111–118, 1978.

[6] J.R. Cave, J.E.Evetts, and A.M. Campbell. Ac flux penetration measurements on force free configuration in reversible type ii superconductor. *Journal de*

Physique (Colloque), 39(C6):614–616, 1978.

[7] J.R. Cave and M.A.R. LeBlanc. Hysteresis losses and magnetic phenomena in oscillating disks of type ii superconductors. *Journal of Applied Physics*, 53(3):1631–1648, 1982.

[8] J.R. Clem. Flux-line-cutting losses in type ii superconductors. *Physical Review*, 26(5):2463–2473, 1982.

[9] J.R. Clem. Spiral vortex instability in type ii superconductors. *Physical Review Letters*, 38:1425–1428, 1977.

[10] J.R. Clem. Steady state flux cutting in type ii superconductors: a double - cutting model. 1986. Ames Laboratory, Iowa State University.

[11] J.R. Clem. Steady state flux-line cutting in type ii superconductors. *Journal of Low Temperature Physics*, 38(3/4):353–369, 1980.

[12] J.R. Clem. Theory of ac losses in type ii superconductors with a field dependent surface barrier. *Journal of Applied Physics*, 50(5):3518–3530, 1979.

[13] J.R. Clem, M.M. Fang, S.L. Miller, J.S. Ostenson, Z.X. Zhao, and D.K. Finnemore. Flux annihilation in superconducting tubes. *Applied Physics Letters*, 47(11):1224–1227, 1985.

[14] J.R. Clem and A. Perez - Gonzalez. Internal magnetic field distribution at the critical current of a type ii superconductors subjected to a parallel magnetic field. *Physical Review B*, 33(3):1601–1609, 1986.

[15] J.R. Clem and A. Perez-Gonzalez. Flux - line cutting and flux pinning in type ii superconductors. In *Proceedings of the International Symposium on Flux Pinning and Electromagnetic Properties of Superconductors*, 1985.

[16] J.R. Clem and S. Yeh. Flux-line-cutting treshold in type ii superconductors. *Journal of Low Temperature Physics*, 39:173–189, 1980.

[17] G. Fillion. *Flux - Line Cutting and Flux Pinning Phenomena in Hollow Cylinder of Type II Superconductor.* PhD thesis, Physics Department, University of Ottawa, 1986.

[18] M.A.R LeBlanc, G. Fillion, and A. Golebiowski. Flux cutting phenomena in a hollow cylinder of a type ii superconductor. *Japanese Journal of Applied Physics*, 26:1509–1510, 1987.

[19] M.A.R LeBlanc, G. Fillion, W.E. Timms, A. Zahradnitsky, and J.R. Cave. Study of the barrier against flux exit from type ii superconductor. *Cryogenics*, 26:491–500, 1981.

[20] J.E. Nicholson and P.T. Sikora. Flux flow in type ii superconducting wires in longitudinal magnetic fields. *Journal of Low Temperature Physics*, 17:275, 1974.

[21] D.J. Walmsley. *Journal of Physics*, F(2):510, 1972.

ABSTRACT

We set out to explore a new approach to reduce axial flux threading the hollow of a superconducting tube by applying and removing an azimuthal magnetic field. To achieve this, we have modified the set up previously used by Fillion. We rebuilt the toroidal magnet coil, increasing the number of turns from 7 of Fillion to 16 and using a different wire capable of carying higher critical current. These changes extended the available range of azimuthal field by a factor of about 3.5 compared to that obtained previously. With this broader range of azimuthal fields, we entered a new domain and encountered a new phenomenon.

We also doubled the turn-area parameter of the inner pick up coil, thereby doubling its sensitivity. Consequently, the reliability and accuracy of our observations of B_z in the hole was correspondingly increased.

By balancing the toroidal pick up coil we improved our ability to monitor the azimuthal magnetization by an order of magnitude and therefore could accurately follow the entry and exit of the azimuthal magnetic flux in the wall simultaneously with the evolution of the axial flux in the hole of the cylinder.

As the applied azimuthal field entered the range of values above 0.2 Tesla, a new and unexpected behaviour was encountered. We present a qualitative interpretation of the two related phenomena observed. Our measurements spanned a wide range of static axial fields. The two characteristics of special interest evolve over this range. In the thesis we display sets of representative data in the low and high axial field regions. These data constitute the first direct evidence for the countermotion of sheets of flux lines.